

PLOS ONE
Prochlorococcus marinus responses to light and oxygen
 --Manuscript Draft--

Manuscript Number:	PONE-D-24-11318
Article Type:	Research Article
Full Title:	Prochlorococcus marinus responses to light and oxygen
Short Title:	Prochlorococcus marinus responses to light and oxygen
Corresponding Author:	Mireille Savoie, MSc. Mount Allison University Sackville, New Brunswick CANADA
Keywords:	Prochlorococcus marinus; dissolved oxygen; photoperiod; growth responses
Abstract:	Prochlorococcus marinus, the smallest picocyanobacterium, comprises multiple clades with distinct niches across tropical and sub-tropical oligotrophic ocean regions, including Oxygen Minimum Zones. Ocean warming may open permissive temperatures in new, poleward photic regimes, along with expanded Oxygen Minimum Zones. We used ocean protein data to help guide testing of Prochlorococcus marinus growth across a matrix of peak irradiances, photoperiods, spectral bands and dissolved oxygen. MED4 from Clade HLI requires greater than 4 h photoperiod, grows at 25 µmol O ₂ L ⁻¹ and above, and exploits high cumulative diel photon doses, yet shows accelerated growth when the cost of photoinactivation is lowered under red, vs. blue, actinic light. MED4 relies upon an alternative oxidase to balance electron transport, which may exclude it from growth under our lowest, 2.5 µmol O ₂ L ⁻¹ , condition. SS120 from Clade LLII/III is restricted to low light under full 250 µmol O ₂ L ⁻¹ , shows expanded light exploitation under 25 µmol O ₂ L ⁻¹ , but is excluded from growth under 2.5 µmol O ₂ L ⁻¹ . Intermediate oxygen suppresses the cost of PSII photoinactivation, and enzymatic production of H ₂ O ₂ in SS120, which has limited genomic capacity for PSII and DNA repair. MIT9313 from Clade LLIV is restricted to low blue irradiance under 250 µmol O ₂ L ⁻¹ , but exploits much higher irradiance under red light, or under lower O ₂ concentrations, conditions which slow photoinactivation of PSII and production of reactive oxygen species.
Order of Authors:	Mireille Savoie, MSc. Aurora Mattison, BSc. Laurel Genge, MSc. Julie Nadeau Sylwia Śliwińska-Wilczewska, PhD. Maximilian Berthold, PhD. Naaman M. Omar, MSc. Ondřej Prášil, PhD. Amanda M. Cockshutt, PhD. Douglas A. Campbell, PhD.
Opposed Reviewers:	
Additional Information:	
Question	Response
Financial Disclosure	Yes
Enter a financial disclosure statement that describes the sources of funding for the work included in this submission. Review	

the [submission guidelines](#) for detailed requirements. View published research articles from [PLOS ONE](#) for specific examples.

This statement is required for submission and **will appear in the published article** if the submission is accepted. Please make sure it is accurate.

Funded studies

Enter a statement with the following details:

- Initials of the authors who received each award
- Grant numbers awarded to each author
- The full name of each funder
- URL of each funder website
- Did the sponsors or funders play any role in the study design, data collection and analysis, decision to publish, or preparation of the manuscript?

Did you receive funding for this work?

Please add funding details.
as follow-up to "[Financial Disclosure](#)"

Enter a financial disclosure statement that describes the sources of funding for the work included in this submission. Review the [submission guidelines](#) for detailed requirements. View published research articles from [PLOS ONE](#) for specific examples.

This statement is required for submission and **will appear in the published article** if the submission is accepted. Please make sure it is accurate.

Czech Academy of Science (OP) visiting fellowship supporting DAC work at AlgaTech
Canada Research Chair in Phytoplankton Ecophysiology (DAC), Grant number CRC-2017-00075

Natural Sciences and Engineering Research Council of Canada, 'Latitude and Light' (DAC)
Canada Foundation for Innovation (DAC)
New Brunswick Innovation Foundation (DAC)
New Brunswick Innovation Foundation STEM Scholarship 2021 and 2022 (MS)
Mount Allison University Rice Graduate Fellowship 2021 and 2022 (MS)

The funders had no role in study design, data collection and analysis, decision to publish, or preparation of the manuscript.

<p>Funded studies</p> <p>Enter a statement with the following details:</p> <ul style="list-style-type: none"> • Initials of the authors who received each award • Grant numbers awarded to each author • The full name of each funder • URL of each funder website • Did the sponsors or funders play any role in the study design, data collection and analysis, decision to publish, or preparation of the manuscript? 	
<p>Did you receive funding for this work?"</p>	
<p>Please select the country of your main research funder (please select carefully as in some cases this is used in fee calculation).</p> <p>as follow-up to "Financial Disclosure"</p> <p>Enter a financial disclosure statement that describes the sources of funding for the work included in this submission. Review the submission guidelines for detailed requirements. View published research articles from PLOS ONE for specific examples.</p>	CANADA - CA
<p>This statement is required for submission and will appear in the published article if the submission is accepted. Please make sure it is accurate.</p>	
<p>Funded studies</p> <p>Enter a statement with the following details:</p> <ul style="list-style-type: none"> • Initials of the authors who received each award • Grant numbers awarded to each author • The full name of each funder • URL of each funder website • Did the sponsors or funders play any role in the study design, data collection and analysis, decision to publish, or preparation of the manuscript? 	
<p>Did you receive funding for this work?"</p>	
<p>Competing Interests</p>	The authors have declared that no competing interests exist.

Use the instructions below to enter a competing interest statement for this submission. On behalf of all authors, disclose any [competing interests](#) that could be perceived to bias this work—acknowledging all financial support and any other relevant financial or non-financial competing interests.

This statement is **required** for submission and **will appear in the published article** if the submission is accepted. Please make sure it is accurate and that any funding sources listed in your Funding Information later in the submission form are also declared in your Financial Disclosure statement.

View published research articles from [PLOS ONE](#) for specific examples.

NO authors have competing interests

Enter: *The authors have declared that no competing interests exist.*

Authors with competing interests

Enter competing interest details beginning with this statement:

I have read the journal's policy and the authors of this manuscript have the following competing interests: [insert competing interests here]

* typeset

Ethics Statement

Enter an ethics statement for this submission. This statement is required if the study involved:

- Human participants
- Human specimens or tissue
- Vertebrate animals or cephalopods
- Vertebrate embryos or tissues

N/A

- Field research

Write "N/A" if the submission does not require an ethics statement.

General guidance is provided below.

Consult the [submission guidelines](#) for detailed instructions. **Make sure that all information entered here is included in the Methods section of the manuscript.**

Format for specific study types

Human Subject Research (involving human participants and/or tissue)

- Give the name of the institutional review board or ethics committee that approved the study
- Include the approval number and/or a statement indicating approval of this research
- Indicate the form of consent obtained (written/oral) or the reason that consent was not obtained (e.g. the data were analyzed anonymously)

Animal Research (involving vertebrate animals, embryos or tissues)

- Provide the name of the Institutional Animal Care and Use Committee (IACUC) or other relevant ethics board that reviewed the study protocol, and indicate whether they approved this research or granted a formal waiver of ethical approval
- Include an approval number if one was obtained
- If the study involved *non-human primates*, add *additional details* about animal welfare and steps taken to ameliorate suffering
- If anesthesia, euthanasia, or any kind of animal sacrifice is part of the study, include briefly which substances and/or methods were applied

Field Research

Include the following details if this study involves the collection of plant, animal, or other materials from a natural setting:

- Field permit number
- Name of the institution or relevant body that granted permission

Data Availability

Authors are required to make all data underlying the findings described fully available, without restriction, and from the time of publication. PLOS allows rare exceptions to address legal and ethical concerns. See the [PLOS Data Policy](#) and [FAQ](#) for detailed information.

Yes - all data are fully available without restriction

<p>A Data Availability Statement describing where the data can be found is required at submission. Your answers to this question constitute the Data Availability Statement and will be published in the article, if accepted.</p> <p>Important: Stating 'data available on request from the author' is not sufficient. If your data are only available upon request, select 'No' for the first question and explain your exceptional situation in the text box.</p> <p>Do the authors confirm that all data underlying the findings described in their manuscript are fully available without restriction?</p>	
<p>Describe where the data may be found in full sentences. If you are copying our sample text, replace any instances of XXX with the appropriate details.</p> <ul style="list-style-type: none"> • If the data are held or will be held in a public repository, include URLs, accession numbers or DOIs. If this information will only be available after acceptance, indicate this by ticking the box below. For example: <i>All XXX files are available from the XXX database (accession number(s) XXX, XXX).</i> • If the data are all contained within the manuscript and/or Supporting Information files, enter the following: <i>All relevant data are within the manuscript and its Supporting Information files.</i> • If neither of these applies but you are able to provide details of access elsewhere, with or without limitations, please do so. For example: <p><i>Data cannot be shared publicly because of [XXX]. Data are available from the XXX Institutional Data Access / Ethics Committee (contact via XXX) for researchers who meet the criteria for access to confidential data.</i></p> <p><i>The data underlying the results presented in the study are available from (include the name of the third party</i></p>	<p>All data obtained from the Multicultivator were saved as comma separated values files and are available at https://github.com/FundyPhytoPhys/prochlorococcus_o2/Data/RawData/MultiCultiData1.zip.</p> <p>https://github.com/FundyPhytoPhys/prochlorococcus_o2/Data/RawData/MultiCultiData2.zip.</p> <p>https://github.com/FundyPhytoPhys/prochlorococcus_o2/Data/RawData/MultiCultiData3.zip. All data obtained from the Jaz spectrometer were saved as text files and are available at https://github.com/FundyPhytoPhys/prochlorococcus_o2/Data/RawData/JazEmData.zip. All data obtained from the Olis 14 UV/VIS Clarity Spectrophotometer were saved as ascii files and are available at https://github.com/FundyPhytoPhys/prochlorococcus_o2/Data/RawData/OlisData.zip. Meta Data for the Multicultivator runs were imported and saved as a .Rds and available at https://github.com/FundyPhytoPhys/prochlorococcus_o2/Data/RawData/CultureCatalog.Rds.</p> <p>Annotated code for data import, transformations and analyses are available at https://github.com/FundyPhytoPhys/prochlorococcus_o2/Code.</p>

(and contact information or URL).

- This text is appropriate if the data are owned by a third party and authors do not have permission to share the data.

* typeset

Additional data availability information:

March 11, 2024

Dear Editor, PLOS ONE.

We submit our manuscript “*Prochlorococcus marinus* responses to light and oxygen” for consideration for publication in PLOS ONE.

In this article, we present the growth responses of 3 *Prochlorococcus marinus* strains; MED4 from Clade HLI, SS120 from Clade LLII/III and MIT9313 from Clade LLIV across a matrix of peak irradiances, photoperiods, spectral bands, and dissolved oxygen. Our study is motivated by evidence of high-light and low-light ecotypes found in ocean regions beyond their optimal habitats, from ocean protein data (<https://www.oceanproteinportal.org/>); coupled with predictions that ocean warming may open permissive temperatures in new, poleward photic regimes, along with expanded Oxygen Minimum Zones. We found that MED4 from Clade HLI requires greater than 4 h photoperiod, grows at 25 $\mu\text{mol O}_2 \text{ L}^{-1}$ and above, and exploits high cumulative diel photon doses. SS120 from Clade LLII/III is restricted to low light under full 250 $\mu\text{mol O}_2 \text{ L}^{-1}$, shows expanded light exploitation under 25 $\mu\text{mol O}_2 \text{ L}^{-1}$, but is excluded from growth under 2.5 $\mu\text{mol O}_2 \text{ L}^{-1}$. MIT9313 from Clade LLIV is restricted to low blue irradiance under 250 $\mu\text{mol O}_2 \text{ L}^{-1}$ but exploits much higher irradiance under red light. MIT9313 demonstrates a tolerance to higher light levels, equivalent to levels used to classify HL clades, under O₂ concentrations of 25 $\mu\text{mol O}_2 \text{ L}^{-1}$ and lower.

We confirm that neither the manuscript nor any parts of its content are currently under consideration or published in another journal. All authors have approved the manuscript and agree with its submission to PLOS ONE.

Sincerely Mireille Savoie,
on behalf of Aurora Mattison, Laurel Genge, Julie Nadeau, Sylwia Śliwińska-Wilczewska,
Maximilian Berthold, Naaman M. Omar, Ondřej Prášil, Amanda M. Cockshutt & Douglas A.
Campbell



1 ***Prochlorococcus marinus* responses to light and oxygen**

2 Mireille Savoie¹, Aurora Mattison^{2,3}, Laurel Genge^{1,4}, Julie Nadeau¹, Sylwia Śliwińska-
3 Wilczewska^{1,5}, Maximilian Berthold¹, Naaman M. Omar¹, Ondřej Prášil^{1,6}, Amanda M.
4 Cockshutt^{2,7}, and Douglas A. Campbell¹

5

6 ¹ Department of Biology, Mount Allison University, Sackville, New Brunswick, Canada

7 ² Department of Chemistry and Biochemistry, Mount Allison University, Sackville, New
8 Brunswick, Canada

9 ³ Department of Biology, University of British Columbia, Vancouver, British Columbia,
10 Canada

11 ⁴ Fisheries and Oceans Canada, Ecosystems Management Branch, Dartmouth, Nova Scotia,
12 Canada

13 ⁵ Institute of Oceanography, University of Gdańsk, Gdańsk, Poland

14 ⁶ Institute of Microbiology, Center Algatech, Laboratory of Photosynthesis, Trebon, Czech
15 Republic

16 ⁷ Department of Chemistry, St. Francis Xavier University, Antigonish, Nova Scotia, Canada

17 **Abstract**

18 *Prochlorococcus marinus*, the smallest picocyanobacterium, comprises multiple
19 clades with distinct niches across tropical and sub-tropical oligotrophic ocean regions,
20 including Oxygen Minimum Zones. Ocean warming may open permissive temperatures in
21 new, poleward photic regimes, along with expanded Oxygen Minimum Zones. We used ocean
22 protein data to help guide testing of *Prochlorococcus marinus* growth across a matrix of peak

23 irradiances, photoperiods, spectral bands and dissolved oxygen. MED4 from Clade HLI
24 requires greater than 4 h photoperiod, grows at 25 $\mu\text{mol O}_2 \text{ L}^{-1}$ and above, and exploits high
25 cumulative diel photon doses, yet shows accelerated growth when the cost of
26 photoinactivation is lowered under red, vs. blue, actinic light. MED4 relies upon an
27 alternative oxidase to balance electron transport, which may exclude it from growth under
28 our lowest 2.5 $\mu\text{mol O}_2 \text{ L}^{-1}$ condition. SS120 from Clade LLII/III is restricted to low light
29 under full 250 $\mu\text{mol O}_2 \text{ L}^{-1}$, shows expanded light exploitation under 25 $\mu\text{mol O}_2 \text{ L}^{-1}$, but is
30 excluded from growth under 2.5 $\mu\text{mol O}_2 \text{ L}^{-1}$. Intermediate oxygen suppresses the cost of PSII
31 photoinactivation, and enzymatic production of H_2O_2 in SS120, which has limited genomic
32 capacity for PSII and DNA repair. MIT9313 from Clade LLIV is restricted to low blue
33 irradiance under 250 $\mu\text{mol O}_2 \text{ L}^{-1}$, but exploits much higher irradiance under red light, or
34 under lower O_2 concentrations, conditions which slow photoinactivation of PSII and
35 production of reactive oxygen species.

36

37

Introduction

38

Prochlorococcus marinus diversity

39 *Prochlorococcus*, a genus of Cyanobacteria, is the smallest known photosynthetic
40 prokaryote, with cell diameters ranging from 0.5 to 0.7 µm [1]. Despite small cell size, *P.*
41 *marinus* contribute 13 to 48% of net primary production in oligotrophic oceans,
42 corresponding to about 30% of global oxygen production [2]. *Prochlorococcus marinus*
43 growth is currently limited to between latitudes of 40°N to 40°S in open ocean waters, from
44 surface to 300 m depth, thus spanning 3 orders of magnitudes of light irradiance [1,2].

45 *Prochlorococcus marinus* comprises many strains, organized into clades, defined by
46 16S-23S intergenic transcribed ribosomal sequence signatures [3]. The clades inhabit
47 distinct ecological niches [4], originally defined as High-Light (HL) or Low-Light (LL). Only 5
48 out of 12 known *Prochlorococcus* genetic clades have cultured representatives to date; HLI,
49 HLII, LLI, LLII/III and LIV [5]. Current niches of *P. marinus* strains span ocean water columns
50 [2,6,7] and extend into regions with low dissolved oxygen concentrations [8–12].

51 Low-Light clades thrive in deeper ocean waters, extending beyond 200 m in depth
52 [2], where only ~1% of the surface irradiance penetrates, primarily in the blue (450 nm) to
53 green (520 nm) spectral range [13]. Clade LLI includes cultured strain NATL2A, which
54 prefers moderate irradiances typical of between 30 and 100 m depth. Clades LLII and LLIII,
55 including cultured strain SS120, are grouped together as the second oldest phylogenetic
56 lineage diversifying in the *P. marinus* radiation, with an affinity for low light. Clade LLIV,
57 including cultured strain MIT9313, falls near the base of the *Prochlorococcus* radiation, and
58 is characterized by preference for low light, typical of depths from 120 m to 200 m [2]. LLIV

59 members are, as yet, the only cultured strains to have been found in Oxygen Minimum Zones
60 (OMZ). Some, as yet, uncultured *P. marinus* strains in clades LLV and LLVI also thrive in OMZ
61 of the subtropical Atlantic and Pacific Oceans, where dissolved oxygen concentrations [O_2]
62 can be less than 20 μM [9–12,14]. *Prochlorococcus marinus* LL ecotypes may indeed
63 dominate the phytoplankton within OMZ [8,10,11], where they may be net O_2 consumers
64 [15].

65 High-Light clades are more recently branching lineages, with reduced genome sizes
66 in comparison to LL clades. High-Light clades are typically dominant picophytoplankters in
67 near-surface, oligotrophic waters, characterized by high light levels and subdivided into
68 clades based on iron adaptation [16–18]. Clade HLI, represented by cultured strain MED4, is
69 adapted to high iron, and low temperatures, and originated from 5 m depth in the
70 Mediterranean Sea [2]. Clade HLII, adapted to high iron, and high temperatures, is the most
71 abundant *P. marinus* clade in the North Atlantic and North Pacific Oceans, often constituting
72 over 90% of the total population [2], and are most numerous around 50 m depth [2]. Clade
73 HLIII/IV is adapted to low iron [16–18].

74 *Prochlorococcus marinus* clades are nonetheless found in environments beyond their
75 optimal habitats. HL clades inhabit depths overlapping with LL ecotypes [17,19,20], while
76 LL clades can occupy regions in OMZ at depths shallower than 40 m [10], exploiting ambient
77 light levels above what LL clades were thought to tolerate.

78 ***Prochlorococcus* and changing niches**

79 Our changing climate is rapidly altering conditions for these specialized clades of
80 marine picophytoplankton. Predictions indicate a net global increase of *P. marinus* cell
81 abundances of 29% [21], along with poleward latitudinal shifts of at least 10° in marine
82 phytoplankton niches by the end of this century [22] in response to warming waters, with
83 increases in *P. marinus* of approximately 50% in the more poleward regions of their
84 distributions.

85 Near the equator, photoperiod remains nearly constant at the ocean surface,
86 approximately 12 hours (h) of daylight and 12 h of darkness throughout the year. The
87 effective length of the photoperiod does, however, attenuate with depth as dawn and dusk
88 light at depth drops below levels needed for biological processes. As *P. marinus* potentially
89 expands its temperature-permissive niches poleward into temperate regions [21,22], it will
90 encounter more pronounced seasonal variations in photoperiod regimes both at surface and
91 at depth, with potentially complex effects upon viable growth niches [23,24]. For example,
92 Vaulot *et al.* [25] showed that *Prochlorococcus* replication of DNA occurs in the afternoon,
93 while cell division occurs at night. To our knowledge, no study has as yet addressed *P.*
94 *marinus* growth responses in relation to a range of photoperiods.

95 Climate change is also rapidly changing ocean chemistry. By the end of this century,
96 surface ocean pH is projected to decline by 0.1 to 0.4 due to projected increases in carbon
97 dioxide concentrations [26]. Moreover, substantial changes in the global water cycle, leading
98 to extensive changes in worldwide precipitation patterns, are affecting ocean salinity levels
99 on a global scale, and ice melts due to rising temperatures are impacting salinity levels in the

100 Arctic and Northwest Atlantic oceans [27]. Increasing sea temperatures are also causing
101 decreases in $[O_2]$ across global oceans [28], particularly toward the poles [29]. Warmer
102 ocean waters decrease oxygen solubility at the surface, and increase stratification, which in
103 turn decreases oxygen mixing downwards by ocean currents [26]. Models predict that OMZ
104 in the Pacific and Indian Oceans are expanding [26,30], although the cores of the OMZ, where
105 the oxygen levels are lowest, may actually contract [30].

106 We used the Ocean Protein Portal (OPP; <https://www.oceanproteinportal.org/>) [31]
107 to analyze the distribution of proteins from clades of *P. marinus* in samples taken across a
108 range of $[O_2]$ and depth, which in turn correlates to depth attenuated peak light at the site of
109 sampling. In parallel we analyzed the growth and physiological responses of representative
110 strains from three clades of *P. marinus* under a matrix of $[O_2]$, light levels, spectral waveband
111 ranges, and photoperiods, to approximate eco-physiological conditions representative of
112 current and hypothetical future ocean zones. *Prochlorococcus marinus* MED4, a clade HLI
113 strain, was isolated near the ocean surface (5m depth) of the Mediterranean Sea where $[O_2]$
114 is near saturation, light levels are high and spectral bias from full solar irradiance is minimal.
115 *Prochlorococcus marinus* SS120, a clade LLII/III strain, was isolated from the Sargasso Sea at
116 a depth of 120 m, while *P. marinus* MIT9313, a clade LLIV strain, was isolated from the North
117 Atlantic Gulf Stream at a depth of 135 m [32]. At these depths, light attenuation and spectral
118 shifts occur, resulting in low blue light, while $[O_2]$ varies from near-surface saturation levels
119 to decreased concentrations, but does not necessarily decrease systematically with depth
120 [33].

121 Photosynthetic organisms absorb light energy within the Photosynthetically Active
122 Radiation (PAR) range, 350 to 700 nm, for photosynthesis [34]. Photosynthetically Usable
123 Radiation (PUR) represents the fraction of PAR that can be absorbed by the pigments of a
124 given photosynthetic organism [34], taking into account the specific spectral wavebands
125 these pigments absorb. *Prochlorococcus marinus* Pcb light-harvesting complexes show an
126 absorption maxima of 442 nm for divinyl chlorophyll *a* and 478 nm for divinyl chlorophyll *b*
127 [35] allowing *P. marinus* to efficiently harvest blue light in the 400 nm to 500 nm range [34]
128 corresponding to blue spectral wavelengths prevailing in deep ocean habitats [13]. In *P.*
129 *marinus* small cell diameters, from 0.5 to 0.7 μm [1], and simple cell structures, minimize the
130 complication of pigment package effect or intracellular self-shading [36] contributing to
131 efficient optical absorption, although photosynthetic efficiency may vary among clades
132 [32,37].

133 Given the different spectral light regimes typical of the niches of different ecotypes,
134 expressing growth rates in terms of cumulative diel PUR might simplify different
135 photoperiods, spectral bands, and PAR levels into a common parameter, making growth
136 response comparisons across strains and different oxygen levels more accessible. We aimed
137 to detect whether growth responses are driven simply by cumulative diel PUR, or whether
138 specific photoperiods, spectral bands or PAR levels have independent, albeit interacting,
139 effects on growth. We therefore analyzed growth rates in terms of cumulative diel PUR.

140 We discuss our findings in relation to analyses of genomic sequences [38] across
141 clades of *P. marinus*, showing that differences in the expression and presence of genes
142 encoding protein turnover, oxygen-dependent enzymes, and DNA repair enzymes, can

143 explain the differential growth responses of strains under the matrix of light and [O₂]

144 conditions of this study.

145

146 **Materials and methods**

147 **Metaproteomics**

148 The Ocean Protein Portal is an open access online data repository (Woods Hole
149 Oceanographic Institution, WHOI) of mass spectroscopy data on marine microbial proteins,
150 sampled from various depths and locations worldwide [31]. We screened a subset of the OPP
151 for proteins annotated as from *Prochlorococcus* strains, to identify differential strategies
152 employed by strains living at varying depths and oxygen levels within the marine water
153 column. We focused on proteins mediating photosynthesis and protein metabolism from
154 depths of 20 to 200 m below the ocean surface. The samples for metaproteomic analyses
155 were collected from 7 locations in the tropical North Pacific Ocean along 150 W from 18 N of
156 the equator between October 1, 2011 and October 25, 2011 during the voyage of the R/V
157 Kilo Moana MetZyme expedition [39]; original datasets in the Biological and Chemical
158 Oceanography Data Management Office (BCO-DMO) repository ([https://www.bco-](https://www.bco-dmo.org/project/2236)
159 [dmo.org/project/2236](https://www.bco-dmo.org/project/2236)) [40]. Oxygen concentration levels at the location of sampling were
160 recorded. The methodology for sample collection and peptide analysis are described by Saito
161 *et al.* [41,42].

162 **Metaproteomics bioinformatic analyses**

163 Metaproteomic datasets were obtained from the KM1128 entry in the BCO-DMO
164 repository [40] accessed via the OPP in June 2019 at [https://www.bco-dmo.org/dataset-](https://www.bco-dmo.org/dataset-deployment/730728)
165 [deployment/730728](https://www.bco-dmo.org/dataset-deployment/730728). This dataset included biomass in the 0.2 to 3.0 micron size
166 fractionated filter size as described in Saito *et al.* [41] where *Prochlorococcus* is found.
167 Datasets contained: i) Protein sequences and sample identification (ID) number; ii) Sample

168 ID number, station, depth in meters below the surface the sample was collected at, best-hit
169 BLASTP protein and species annotation and the corresponding Uniprot Entry number for
170 the identified proteins; iii) Sample station depth and [O₂].
171 The depth and [O₂] (also from BCO-DMO at <https://www.bco-dmo.org/dataset/646115/>)
172 were joined to protein sequence and BLASTP annotations by ID number, depth and station
173 using *tidyverse* package [43] running under R v4.1.3 and RStudio v2023.06.0 [44]. The
174 resulting merged dataset was filtered for those *Prochlorococcus* protein, detected from 0 to
175 300 m below the surface, annotated as a subunit of *Prochlorococcus* chlorophyll binding
176 proteins (Pcb); Photosystem II (PSII); Cytochrome b₆f (Cytb₆f); Photosystem I (PSI);
177 NADPH Dehydrogenase (NDH); Plastoquinol Terminal Oxidase (PTOX); Plastocyanin (PC);
178 Ferredoxin (Fd); Ribulose-1,5-bisphosphate oxygenase (RUBISCO); Adenosine
179 triphosphate (ATP) Synthase; FtsH proteases (FtsH) or ribosomes. Detected peptides were
180 re-annotated for consistency and labelled, where feasible, according to strain, clade,
181 subunit and protein complex. Full protein sequences corresponding to detected proteins
182 were obtained from UniProt (<https://www.uniprot.org/>) and analyzed in Molecular
183 Evolution and Genetic Analyses X (MEGAX) software (<https://www.megasoftware.net/>).
184 Sequences for proteins for each of the thirteen *Prochlorococcus* strains identified in the
185 dataset were aligned with MUSCLE using UPGMA cluster method and a lambda of 24 with a
186 -2.9 gap open penalty and 1.20 hydrophobicity multiplier. Overall mean pairwise distance
187 between protein sequences was determined using bootstrap variance estimation methods.
188 Maximum likelihood phylogenetic trees were assembled using 1000 bootstrap replications
189 with a 95% site coverage cut off. *Prochlorococcus* FtsH isoform identities, and functions,
190 were inferred by sequence comparisons to the characterized four isoforms of FtsH

191 protease of *Synechocystis* sp. PCC6803 [45]. Data for each strain was plotted against depth
192 and [O₂] and sampling station.

193 When assessing the presence of a particular protein complex at a sampling location,
194 the spectral counts were summed between proteins within the protein subunit to give the
195 greatest number of data points. As this data was acquired by survey proteomics (data
196 dependent acquisition) rather than through targeted peptide approaches (e.g. parallel
197 reaction monitoring), it is difficult to discern accuracies of strain assignment annotations,
198 particularly as the proteins of interest in this study are highly conserved across strains [42].
199 We are, however, confident in clade classifications for each protein examined. The data is
200 also limited because a peptide sequence was not determined unless there was already a
201 known spectrum for that peptide in the SEQUEST database, hence some peptides of interest
202 may not be identifiable. This MetZyme dataset used a deep paired metagenomic database
203 (<https://www.ebi.ac.uk/pride/archive/projects/PXD030684>) to enable this peptide-to-
204 spectrum matching [41,46]. Furthermore, protein identifications were based on peptide to
205 spectrum matching using SEQUESTHT within Proteome Discoverer software (Thermo) and
206 spectral counts were enumerated using Scaffold software (Proteome Software) using a FDR
207 of <0.1% on the peptide level as described in Saunders *et al.* [47].

208 ***Prochlorococcus* culturing and experimental design**

209 *Prochlorococcus* remain challenging to culture, as their reduced genomes – the
210 smallest of any known oxyphototroph – render them partially dependent upon mutualistic
211 heterotrophic bacteria to detoxify reactive oxygen species [48,49]. MED4, SS120 and
212 MIT9313 have been successfully cultured in laboratories [50,51], and used to show that

213 ecotypic classifications correspond to biochemical differences among strains [45]. Three
214 xenic cultures of *P. marinus* were obtained from Bigelow Labs, NCMA Maine, USA. MED4
215 (CCMP1986) is from High-Light adapted (HLI) clade; SS120 (CCMP1375) is from Low-Light
216 adapted (LLII/III) clade; and MIT9313 (CCMP2773) is from Low-Light adapted (LLIV) clade.
217 Cultures were maintained in incubators set to 22°C with an on/off light/dark cycle of 12 h.
218 The PAR level for maintenance cultures reflected PAR in the source niche of the ecotype;
219 MED4, of 160 $\mu\text{mol photons m}^{-2} \text{s}^{-1}$ with illumination from STANDARD Products Inc. Cool
220 White F24T5/41K/8/HO/PS/G5/STD, 24 watts, fluorescent bulbs; SS120 and MIT9313 at
221 30 $\mu\text{mol photons m}^{-2} \text{s}^{-1}$ with illumination from Philips Cool White F14T5/841 Alto, 14 watts,
222 fluorescent bulbs. To maintain active growth all strains were transferred weekly with 1 in 5
223 dilutions with Pro99 media [51] prepared with autoclaved artificial seawater [52].

224 Controlled growth experiments were performed using MCMIX-OD or MC1000-OD PSI
225 Multicultivators (S1 Fig.; PSI, Drásov, Czech Republic). Each multicultivator individually
226 controls 8 tubes at a common temperature of 22°C. Each tube containing 70 mL of Pro99
227 media was inoculated with 10 mL of growing maintenance culture. In a factorial matrix
228 design, each tube was then subject to an individual combination of sinusoidal photoperiod
229 (4, 8, 12, 16 h); reaching a peak PAR (30, 90, 180 $\mu\text{mol photons m}^{-2} \text{s}^{-1}$), with defined spectral
230 bandwidth (White LED, 660 nm, 450 nm). $[O_2]$ levels (2.5 μM , 25 μM , 250 μM) were imposed
231 by bubbling tubes with varying ratios of air and Nitrogen (N_2), with consistent 0.05% of
232 Carbon Dioxide (CO_2) gas, delivered through a 0.2 μm sterile microfilter via a G400 gas
233 mixing system (Qubit Systems Inc., Kingston, Ontario, Canada). $[O_2]$ *in situ* was verified using
234 oxygen optodes (PyroScience, Germany) inserted into tubes for real-time measurements,

235 with a temperature probe in the bath of the bioreactor to correct [O₂] measures for
236 temperature fluctuations. In addition, the Pyroscience software corrected [O₂] based on the
237 salinity of the media (32 ppt). The flow rate of the gas mixture was controlled, but variations
238 in bubbling speed, PAR and culture density affected the [O₂] achieved in each tube. A low [O₂]
239 of 0.5 µM - 5 µM (reported as 2.5 µM hereafter), was achieved by sparging with a gas mixture
240 containing 99.95% N₂ and 0.05% CO₂. An intermediate [O₂] of 10 - 25 µM (reported hereafter
241 as 25 µM) was achieved by sparging with a gas mixture containing 98.95% N₂, 0.05% CO₂
242 and 1% O₂. A high O₂ of 200 µM - 280 µM (reported hereafter as 250 µM) was achieved by
243 sparging with lab air (78% N₂, 21% O₂, 1% Ar and 0.05% CO₂).

244 The full crossing of all factor levels would yield 4 x 3 x 3 x 3 = 108 treatments, x 3
245 strains for 324 possible combinations. Consistent absence of growth of some strains under
246 some levels of photoperiod, PAR, or [O₂] meant we completed 268 growth factor treatment
247 combinations.

248 *In situ* measurements of Optical Density (OD) 680 nm, a proxy for cell suspension
249 density, cell size dependent scatter and cell chlorophyll content; and OD 720 nm, a proxy for
250 cell suspension density and cell size dependent scatter, were recorded every 5 minutes over
251 least 8 to 14 days, depending on the duration of the lag phase, if any.

252 Peak PAR of 180, 90 or 30 µmol photons m⁻² s⁻¹, and spectral wavebands (white LED
253 full spectrum, 660 nm (red light), and 450 nm (blue light)) were chosen to approximate light
254 levels and spectral colours spanning the vertical ocean water column, from near-surface to
255 the lower euphotic zone depths. Photoperiods were chosen to approximate diel cycles

256 characteristic of current and hypothetical future niches of *P. marinus*; 16 h represents
257 temperate (45°N) summer at the ocean surface; 12 h for equatorial (0°N) ocean surface or
258 temperate (45°N) spring and fall ocean surface or temperate (45°N) summer at deeper ocean
259 depths; 8 h for temperate (45°N) winter at the surface or at temperate (45°N) spring and fall
260 at depth and equatorial (0°N) deep ocean depths; and 4 h for temperate (45°N) winter or
261 deep ocean depths during temperate (45°N) spring and fall.

262 **Growth rate analysis**

263 Data files (.csv) saved from the Multicultivator software were imported into R-Studio
264 for data management [43], growth rate calculations, comparisons of model fits [53], and
265 visualization. The chlorophyll proxy optical density ($OD_{680} - OD_{720}$; ΔOD) was used to
266 determine the chlorophyll specific growth rate (μ , d^{-1}) for each treatment combination. We
267 first used a rolling mean from the R package *zoo* [54] to calculate the average ΔOD data over
268 a 1-hour window to lower the influence of outlier points and remove data points collected
269 during post stationary phase, when applicable. We used the Levenberg-Marquardt algorithm
270 [55] modification of the non-linear least squares, using the R package *minpack.lm* [56], to fit
271 a logistic equation (Equation (1)); where ΔOD_{max} is maximum ΔOD , ΔOD_{min} is minimum ΔOD ,
272 t is time duration over the growth trajectory.

$$273 \quad \mu = \frac{\Delta OD_{max} \times \Delta OD_{min} \times \exp^{(\mu \times t)}}{\Delta OD_{max} + (\Delta OD_{min} \times \exp^{((\mu \times t) - 1)})} \quad (1)$$

274 S2 Fig. is an example of chlorophyll specific growth estimates fitted from the high
275 resolution ΔOD measurements for each tube in a Multicultivator. The residuals of the logistic

276 growth curve fit are shown. The imposed PAR ($\mu\text{mol photons m}^{-2} \text{ s}^{-1}$) are plotted for each
277 tube and illustrates the applied photoperiod (h) regimes.

278 A Generalized Additive Model (GAM) [57] was applied to the relation of chlorophyll-
279 specific μ, d^{-1} to photoperiod and PAR level, for each growth [O_2] level, and for the blue and
280 red wavebands for growth, for each *P. marinus* strain in this study. The R package *mgcv* [58]
281 was used to model the growth rate with smoothing terms and indicate the 90, 50 and 10%
282 quantiles for growth rate across the levels of factors. Only growth rate estimates for which
283 the amplitude of standard error was smaller than 30% of the fitted growth rate were
284 included in the GAM. Our priority was the effects of ecologically relevant blue light on growth
285 trends. We also included GAM analyses of growth responses to red light, which is not
286 ecophysiological relevant, but which might prove mechanistically informative [59].

287 **Estimation of photosynthetically usable radiation**

288 To estimate the Photosynthetically Usable Radiation (PUR), a proxy of incident
289 photons that can be absorbed by the cells, for each *P. marinus* ecotype, the imposed
290 Photosynthetically Active Radiation (PAR) was first determined using the reported delivery
291 of sinusoidal diel PAR regimes by the Multicultivators, point validated using a LI-250
292 quantum sensor (LI-COR Inc., Lincoln, NE, USA). An emission profile from 400 nm to 700 nm
293 of each coloured LED light of the MCMIX-OD Multicultivator and the white LED light of the
294 MC1000-OD Multicultivator was obtained using a Jaz spectrometer (Ocean Optics,
295 Inc., Dunedin, FL, USA) equipped with a fiber optic cable, HH2 FiberOpticJmp (Part number
296 A901073, Malvern Panalytical Ltd, Malvern, UK). Each LED spectrum was then normalized
297 to its emission maximum. An *in-vivo* whole cell absorbance spectrum for each *P. marinus*

298 strain under each spectral growth condition was obtained using the Olis 14 UV/VIS Clarity
299 Spectrophotometer (Olis Inc., Bogart, GA, USA) to scan across range of $\lambda = 350$ nm to 750 nm
300 at 1 nm intervals. The path length of the internally reflective cavity of the Olis
301 spectrophotometer was corrected to a 1 cm path length using the Javorfi correction method
302 [60] on PRO 99 media subtracted whole cell absorbance spectra. The blank-corrected whole
303 cell absorbance spectra were normalized to the absorbance maximum of divinyl chlorophyll
304 *a* (Chl *a*₂), determined for each spectra, falling between 400 nm and 460 nm.

305 An integrated weighting equation (2) [34] was used to determine the weighted PUR
306 spectrum $P(\lambda)$; where $A(\lambda)$ is the blank subtracted, Chl *a*₂ peak normalized whole cell
307 absorbance spectrum for each *P. marinus* ecotype, over 400 nm to 700 nm, $A(\lambda)$; and $E(\lambda)$ is
308 the peak normalized emission spectrum of the imposed LED growth light, over 400 nm to
309 700 nm.

310
$$P(\lambda) = A(\lambda) \times E(\lambda) \quad (2)$$

311 PUR levels ($\mu\text{mol photons m}^{-2} \text{s}^{-1}$) were calculated from imposed PAR ($\mu\text{mol photons}$
312 $\text{m}^{-2} \text{s}^{-1}$) levels using the equation (3) from [34]; where $P(\lambda)$ is the weighted PUR absorbance
313 spectrum from equation (2), $E(\lambda)$ is the imposed growth light emission spectrum from
314 equation (2) and PAR is the imposed peak light level ($\mu\text{mol photons m}^{-2} \text{s}^{-1}$). Fig. (1) shows
315 the calculated peak PUR ($\mu\text{mol photons m}^{-2} \text{d}^{-1}$) vs. imposed peak PAR ($\mu\text{mol photons m}^{-2} \text{s}^{-1}$
316 $)$ for each strain and each spectral waveband (nm).

317
$$PUR = \frac{\int_{400}^{700} P(\lambda)}{\int_{400}^{700} E(\lambda)} \times PAR \quad (3)$$

318 The applied photoperiods were delivered using the sinusoidal circadian light function
319 of the PSI Multicultivator to simulate light exposure approximating sun rise through to
320 sunset. The area under the sinusoidal curves is equivalent to the area of a triangular
321 photoregime of equivalent photoperiod (Campbell, unpub), therefore the equation to
322 determine the cumulative diel PUR ($\mu\text{mol photons m}^{-2} \text{ d}^{-1}$) is one half of the base
323 (photoperiod) multiplied by the height (PUR) (Equation (4)); where PUR is the usable light
324 ($\mu\text{mol photons m}^{-2} \text{ s}^{-1}$) calculated from equation (3), 3600 is the time conversion from
325 seconds to hour and photoperiod is the imposed photoperiod (h).

326
$$\text{Cumulative diel PUR} = \frac{\text{PUR} \times 3600 \times \text{Photoperiod}}{2} \quad (4)$$

327 S3 Fig. provide visual representations of PUR, the black solid line and shaded area, in
328 relation to the imposed PAR, the dotted line, under each imposed spectral wavebands for *P.*
329 *marinus* MED4 (A-C), SS120 (D-F) and MIT9313 (G-I). Fig. (1) shows the relationship
330 between calculated PUR vs. imposed PAR for each *P. marinus* and each spectral waveband.

331 We performed one-way ANOVA to examine statistical differences between Harrison
332 and Platt [53] 4 parameter model fit to 660 nm (red light) and 450 nm (blue light) growth
333 data for each combination of strain and $[O_2]$. We also performed one-way ANOVA to examine
334 statistical differences between Harrison and Platt [53] 4 parameter model fit to each
335 photoperiod (4 h, 8 h, 12 h, 16 h) and pooled photoperiod growth data for each combination
336 of strain and $[O_2]$. Photoperiod growth data that showed complete growth inhibition for each
337 combination of strain, $[O_2]$ and imposed spectral waveband were omitted from the pooled
338 photoperiod model. Statistical differences were determined at P value < 0.05 .

339 *Fig. 1: Peak Photosynthetically Usable Radiation (PUR; $\mu\text{mol photons m}^{-2} \text{s}^{-1}$) vs. peak*
340 *Photosynthetically Active Radiation (PAR; $\mu\text{mol photons m}^{-2} \text{s}^{-1}$). The correlation between*
341 *PAR, plotted on the x-axis and PUR, plotted on the y-axis, are coloured for each imposed spectral*
342 *waveband; 450 nm (blue circles), 660 nm (red circles) and white LED (black circles). The grey*
343 *dashed line represents a hypothetical one to one correlation. A. is Prochlorococcus marinus*
344 *MED4. B. is Prochlorococcus marinus SS120. C. is Prochlorococcus marinus MIT9313.*

345

346 ***Prochlorococcus* comparative genomics**

347 We filtered the dataset of Omar *et al.* [61], for Enzyme Commission Numbers (EC
348 numbers), or Kegg Orthology Numbers (KO numbers) identified by BRENDA [38] as ‘natural
349 substrates’ for O₂; EC numbers identified by BRENDA as being activated, or inhibited by light;
350 and EC numbers annotated by BioCyc [62] as corresponding to the Gene Ontology Term
351 ([GO:0006281](#) - DNA repair), in *P. marinus* strains (MED4, MIT9313, SS120, and NATL2A). We
352 grouped orthologs together by EC number and their KO number and determined the
353 occurrences of individual orthologs encoding each EC number, or KO number when EC
354 number was not available, in a given strain. We merged the dataset with a list of enzyme
355 Michaelis constant (K_m) values from other organisms, as K_m values from *Prochlorococcus*
356 were only available in the case of Ribulose bisphosphate carboxylase. Gene counts for
357 Flavodiirons were obtained from Allahverdiyeva *et al.* [63], as they do not have allocated EC
358 numbers. A full list of enzymes and corresponding EC and KO numbers can be found in S1
359 Table.

360

361 **Results and discussion**

362 **Detection of *Prochlorococcus* proteins across O₂ and light niches in the ocean**

363 Proteins from 13 annotated strains of *P. marinus* were detected across depths and
364 oxygen concentrations in the ocean proteins data set analyzed. We focused our analysis here
365 on core photosynthetic protein complexes, for clades HL, LLI, LLII/III and LLIV (Fig. 2) as a
366 function of depth (a proxy for light intensity) and measured [O₂]. Photosynthetic complexes
367 from HLI (including strain MED4) were detected throughout the water column,
368 predominantly at high [O₂]. The absence of proteins annotated for the key ATP Synthase
369 complex for Clade HLI, compared to annotated detections of ATP Synthase across the other
370 three clades suggests limitations in the annotation process for highly conserved protein
371 sequences. Complexes from Clades LLI (including strain NATL2A) were also present across
372 the depth/light axes, with more representation at lower [0~2], and fewer near surface
373 detections. Complexes from clade LLII/III (ex. SS120) were also detected across the
374 depth/light and [O₂] ranges, with more detections at deeper, darker depths. Clade LLIV (ex.
375 MIT9313) photosynthetic complexes were also were detected throughout the depth/light
376 and [O₂], ranges, with the most frequent detections at depth and at low [O₂], compared to
377 other strains.

378

380 *Fig. 2: Ocean detection of Prochlorococcus marinus photosynthesis complexes.* Protein
381 detections (circles) are plotted vs. O_2 (μM) (X-axis) and depth (m) (Y-axis) at sample origin.
382 Rows separate data annotated as from Prochlorococcus clades: HLI (including *P. marinus*
383 MED4, solid black circles), LLI (including *P. marinus* NATL2A, solid black circles), LLII/III
384 (including *P. marinus* SS120, solid black circles) and LLIV (including *P. marinus* MIT9313, solid
385 black circles). Columns show detections of proteins annotated as Photosystem II (PSII),
386 Cytochromeb6f complex (Cytb6f), Photosystem I (PSI), ATP Synthase or Ribulose-1,5-
387 bisphosphate oxygenase carboxylase (RUBISCO). For comparison culture growth experimental
388 conditions are indicated by horizontal grey lines for depths approximating peak
389 Photosynthetically Active Radiation (PAR; μmol photons $m^{-2} s^{-1}$); and vertical grey lines for
390 imposed $[O_2]$ (μM). Data obtained from the Biological and Chemical Oceanography Data
391 Management Office repository [40].

393 ***Prochlorococcus marinus* growth responses to photoperiod, PAR, spectral band,
394 and [O₂]**

395 Guided in part by the evidence of ocean distributions of proteins from
396 *Prochlorococcus* we set up a matrix of photoperiods, PAR, spectral bands, and [O₂] to
397 approximate current, and potential future, latitudinal, depth and seasonal niches for
398 *Prochlorococcus* strains. As mentioned, growth under red light could prove mechanistically
399 informative [59] to factors limiting *Prochlorococcus* growth, we therefore included the red
400 spectral waveband even though it is not representative of *Prochlorococcus* niches. Although
401 *Prochlorococcus* is currently limited to a narrow range of surface photoperiods, potential
402 poleward latitudinal expansions, in combination with attenuation of light with depth, mean
403 *Prochlorococcus* may potentially encounter a wide range of photoperiods. Our growth rate
404 determinations generally agree with those from Moore *et al.* [50], for white LED and 250 μM
405 O₂, but our study is, to our knowledge, the first to analyze the interactive growth responses
406 of *Prochlorococcus* strains to varying [O₂], spectral wavebands and photoperiods.

407 *Prochlorococcus marinus* MED4, clade HLI, growth under 250 μM O₂ increased with
408 higher imposed PAR and longer photoperiods (Fig. 3), across all spectral wavebands. No
409 growth was observed under any imposed conditions under a 4 h photoperiod. The maximum
410 growth rate (μ_{\max}) was 0.68 d⁻¹ achieved under 180 μE blue light and 16 h photoperiod.

411 Similar to growth trends under 250 μM O₂, MED4 maintained at 25 μM O₂ showed
412 fastest growth when the photoperiod was 16 h for each spectral waveband, across PAR levels
413 (Fig. 3). The μ_{\max} was 0.65 d⁻¹ (S2 Table) achieved under 180 μmol photons m⁻² s⁻¹ blue light
414 and 16 h photoperiod. The 4 h photoperiod experiments under white LED light were not

415 performed as no growth was achieved when grown under an 8 h photoperiod of white LED
416 light.

417 MED4 did not grow when sparged to the lowest [O₂] of 2.5 μM (Fig. 3). 2.5 μM O₂
418 growth experiments were not conducted for 4 and 16 h photoperiods, as no reproducible
419 growth occurred when MED4 was exposed to 8 and 12 h photoperiods.

420

421

422 *Fig. 3: Chlorophyll specific growth rate (d^{-1}) for *Prochlorococcus marinus MED4 (High-**

423 *Light (HLI) near surface clade) vs. photoperiod (h).* Rows separate data from levels of

424 *imposed dissolved O₂ concentrations (250 μ M, 25 μ M and 2.5 μ M). Columns separate data from*

425 *3 levels of peak imposed Photosynthetically Active Radiation (PAR; 30, 90 and 180 μ mol*

426 *photons m⁻² s⁻¹). Colours represent the imposed spectral waveband (nm). Large circles show*

427 *mean or single determinations of growth rate from logistic curve fits; small circles show values*

428 *for replicate determinations, if any: replicates often fall with larger circles.*

429

430 The GAM model in Fig. 4 summarizes MED4 growth responses to red (A and B) or
431 blue (C and D) peak PAR and photoperiod across 2 imposed oxygen concentrations. Under
432 250 μM O_2 MED4 achieved fastest growth rates above peak blue light of $\sim 180 \mu\text{mol}$ photons
433 $\text{m}^{-2} \text{s}^{-1}$, and the longest photoperiod of 16, indicated by the 0.64 d^{-1} contour line representing
434 the 90th percentile of maximum achieved growth rate (Fig. 4C). Growth decreased with
435 decreasing photoperiod and decreasing peak PAR. Under red light growth was generally
436 slower but the pattern of growth responses to photoperiod and PAR was similar (Fig. 4A).
437 Note the exclusion of MED4 from growth under 4 h photoperiod under both red and blue
438 light (Fig. 4). Under 25 μM O_2 MED4 showed similar growth responses, but was excluded
439 from both 4 and 8 h photoperiods. MED4 did not grow under 2.5 μM O_2 , so no GAM model
440 was run. Considering the range of PAR levels, and spectral bands that MED4 can utilize,
441 MED4 can inhabit not just shallow depths, where light levels are high, but also deeper
442 regions, characterized by a lower level of blue light, subject to the limitation of a photoperiod
443 of more than 4 h, even after depth attenuation of light. The photoregimes of winter temperate
444 zones, due to shorter photoperiods, exclude MED4 from growth at any depth, however
445 temperate photoperiods and light levels for the remainder of the year are potentially
446 adequate to support MED4 growth, if water temperatures warm into the clade HLI tolerance
447 range.

448

449

450 *Fig. 4: A contour plot of a Generalized Additive Model (GAM) representing the chlorophyll*
451 *specific growth rate (d^{-1}) for Prochlorococcus marinus MED4 grown under 660 nm (red)*
452 *or 450 nm (blue) light. X-axis is photoperiod (h). Y-axis is Photosynthetically Active*
453 *Radiation (PAR, $\mu\text{mol photons m}^{-2} \text{s}^{-1}$). A. represents the model under 250 μM of O_2 and red*
454 *light. B. represents the model under 25 μM of O_2 and red light. C. represents the model under*
455 *250 μM of O_2 and blue light. D. represents the model under 25 μM of O_2 and blue light. Legends*
456 *represent a colour gradient of growth rate from no growth (white) to 1.00 d^{-1} (dark red or dark*
457 *blue). Labeled contour lines indicate the 90%, 50%, and 10% quantiles for achieved growth*
458 *rate.*

459

460 *Prochlorococcus marinus* SS120 clade LLII/III, growth under 250 μM O_2 increased
461 with longer photoperiods, under 30 μmol photons $\text{m}^{-2} \text{s}^{-1}$ peak PAR and across all spectral
462 wavebands (Fig. 5). No growth was observed under any blue light photoperiods when
463 exposed to peak PAR of 90 μmol photons $\text{m}^{-2} \text{s}^{-1}$ or greater. Growth rate, however increased
464 with increasing photoperiods for white and red light under peak PAR of 90 μmol photons $\text{m}^{-2} \text{s}^{-1}$
465 but showed growth inhibition at 16 h red light photoperiod. Growth rate decreased with
466 longer photoperiods and showed growth inhibition at 12 and 16 h photoperiods under PAR
467 of 180 μmol photons $\text{m}^{-2} \text{s}^{-1}$ white LED, red or blue light. The μ_{max} was 0.5 d^{-1} (S2 Table)
468 achieved under 90 μmol photons $\text{m}^{-2} \text{s}^{-1}$ white LED light and 16 h photoperiod.

469 Under 25 μM O_2 and PAR of 30 μmol photons $\text{m}^{-2} \text{s}^{-1}$ growth trends were similar to
470 250 μM O_2 . SS120 showed no growth under a 4 h photoperiod for red spectral waveband,
471 however under blue light, SS120 was able to grow (Fig. 5). In contrast to the growth trends
472 of the 250 μM O_2 and PAR of 90 μmol photons $\text{m}^{-2} \text{s}^{-1}$ experiments, SS120 grew under 4 and
473 8 h blue light and 16 h red light photoperiods, however the growth rate decreased under 12
474 and 16 h white LED light photoperiod treatments. Blue light treatments under PAR of 180
475 μmol photons $\text{m}^{-2} \text{s}^{-1}$ showed growth only under an 8 h photoperiod. The μ_{max} was 0.45 d^{-1}
476 (S2 Table) achieved under 90 μmol photons $\text{m}^{-2} \text{s}^{-1}$ blue light and 8 h photoperiod. The 25
477 μM O_2 , less than 16 h photoperiod and 180 μmol photons $\text{m}^{-2} \text{s}^{-1}$ under white LED light
478 experiments were not performed due to time constraints.

479 SS120 did not reproducibly grow when sparged to the lowest O_2 of 2.5 μM (Fig. 5). 2.5
480 μM O_2 growth experiments were not conducted for 4 and 16 h photoperiods under PAR of
481 180 μmol photons $\text{m}^{-2} \text{s}^{-1}$, as no growth occurred when SS120 was exposed to 8 and 12 h

482 photoperiods. Red light 16 h photoperiod experiments were not performed due to time
483 constraints.

484

485 *Fig. 5: Chlorophyll specific growth rate (d^{-1}) for Prochlorococcus marinus SS120 (Low-*
486 *Light (LLII/III) deep ocean clade) vs. photoperiod (h).* Rows separate data from levels of
487 imposed dissolved O_2 concentrations (250 μM , 25 μM and 2.5 μM). Columns separate data from
488 3 levels of peak imposed Photosynthetically Active Radiation (PAR; 30, 90 and 180 μmol
489 photons $m^{-2} s^{-1}$). Colours represent the imposed spectral waveband (nm). Large circles show
490 mean or single determinations of growth rate from logistic curve fits; small circles show values
491 for replicate determinations, if any: replicates often fall with larger circles.

492

493 The GAM model in Fig. 6 summarizes growth responses of SS120 to red (A and B) or
494 blue (C and D) peak PAR and photoperiod, across the 2 imposed oxygen concentrations.
495 Under 250 $\mu\text{M O}_2$, Fig. 6C showed highest growth rates below blue light PAR of 50 μmol
496 photons $\text{m}^{-2} \text{s}^{-1}$ and photoperiods between 8 and 12 h, indicated by the contour line labeled
497 0.18 d^{-1} (representing the 90th percentile of achieved growth rate). Under 250 $\mu\text{M O}_2$ SS120
498 is constrained to deeper ocean waters through its intolerance of higher blue PAR levels.
499 These findings align with Moore *et al.* [50] and are expected for a low light clade. The disjunct
500 regions of the GAM plot results from variable growth success of SS120 under 250 $\mu\text{M O}_2$.
501 Growth rate patterns under red light were similar, although somewhat faster. In contrast,
502 under 25 $\mu\text{M O}_2$ and a photoperiod of 8 h SS120 exploited all blue peak PAR levels, achieving
503 faster growth rates at a higher PAR of $\sim 100 \mu\text{mol photons m}^{-2} \text{s}^{-1}$, indicated by the contour
504 line labeled 0.41 d^{-1} (representing the 90th percentile of achieved growth rate), outpacing
505 the 90th percentile fastest growth rates under 250 $\mu\text{M O}_2$ (Fig. 6D). Under red light and 25
506 $\mu\text{M O}_2$ (Fig. 6B) SS120 grew across most conditions of peak PAR and photoperiod, achieving
507 fastest growth under long photoperiods and peak PAR between 30 $\sim 100 \mu\text{mol photons m}^{-2}$
508 s^{-1} . Thus, the designation of SS120 as a LL strain is dependent upon the $[\text{O}_2]$. SS120 did not,
509 however, grow reliably under tested conditions at 2.5 $\mu\text{M O}_2$.

510

511

512 *Fig. 6: Contour plot of a Generalized Additive Model (GAM) representing the chlorophyll*
513 *specific growth rate (d^{-1}) for Prochlorococcus marinus SS120 grown under 660 nm (red)*
514 *or 450 nm (blue) light. X-axis is photoperiod (h). Y-axis is Photosynthetically Active*
515 *Radiation (PAR, $\mu\text{mol photons m}^{-2} \text{s}^{-1}$). A. represents the model under 250 μM of O_2 and red*
516 *light. B. represents the model under 25 μM of O_2 and red light. C. represents the model under*
517 *250 μM of O_2 and blue light. D. represents the model under 25 μM of O_2 and blue light. Legends*
518 *represent a colour gradient of growth rate from no growth (white) to 1.00 d^{-1} (dark red or dark*
519 *blue). Labeled contour lines indicate the 90%, 50%, and 10% quantiles for achieved growth*
520 *rate.*

521

522 *Prochlorococcus marinus* MIT9313, clade LLIV, growth under 250 μM O_2 increased
523 with longer photoperiods, under low 30 μmol photons $\text{m}^{-2} \text{s}^{-1}$ peak PAR, (Fig. 7). Under
524 intermediate 90 μmol photons $\text{m}^{-2} \text{s}^{-1}$ peak PAR growth rates decreased with increasing blue
525 light photoperiods. Blue light did not induce growth at 180 μmol photons $\text{m}^{-2} \text{s}^{-1}$ peak PAR,
526 while MIT9313 showed only marginal growth under white LED and red light at 180 μmol
527 photons $\text{m}^{-2} \text{s}^{-1}$ peak PAR, under the 8 h photoperiod, consistent with Moore *et al.* [32]. The
528 μ_{\max} was 0.54 d^{-1} achieved under 30 μmol photons $\text{m}^{-2} \text{s}^{-1}$ blue light and 16 h photoperiod.

529 For MIT9313 under 25 μM O_2 , growth rate increased with increasing photoperiods
530 for all spectral wavebands tested (Fig. 7), with the fastest overall growth rate for MIT9313
531 1.01 d^{-1} achieved under peak PAR of 90 μmol photons $\text{m}^{-2} \text{s}^{-1}$ and 16 h white LED light
532 photoperiod. In marked contrast to the 250 μM O_2 growth experiments, MIT9313 grew when
533 exposed to peak PAR of 180 μmol photons $\text{m}^{-2} \text{s}^{-1}$ and blue light under all photoperiods
534 except 16 h; additionally, white LED and red light treatments induced growth across all
535 tested photoperiods under 25 μM O_2 . The 25 μM O_2 , 4 h photoperiod experiments under
536 white LED light and were not performed due to time constraints.

537 MIT9313 grew under 2.5 μM O_2 particularly under blue LED light, albeit generally
538 slower than under the parallel experiments at 25 μM O_2 (Fig. 7). Growth estimates showed
539 scatter among replicates, suggesting 2.5 μM O_2 is near the tolerance limit for growth of
540 MIT9313. Growth rates increased with longer photoperiods under blue light treatments and
541 peak PAR of 90 μmol photons $\text{m}^{-2} \text{s}^{-1}$ but did not grow under 16 h photoperiod. Growth for
542 MIT9313 under PAR of 180 μmol photons $\text{m}^{-2} \text{s}^{-1}$ and blue light treatment decreased with
543 increasing photoperiods with full growth inhibition under a 16 h photoperiod. The red light

544 peak PAR of 180 $\mu\text{mol photons m}^{-2} \text{s}^{-1}$ showed similar growth rates to blue light for 8 and 12
545 h photoperiods. The μ_{max} was 0.45 d^{-1} achieved under 12 h blue light photoperiod and PAR
546 of 90 $\mu\text{mol photons m}^{-2} \text{s}^{-1}$. The 2.5 $\mu\text{M O}_2$ white LED treatments under 4, 8 and 16 h
547 photoperiods and red light under 4 and 16 h photoperiods were not performed due to time
548 constraints.

549

550

551 *Fig. 7: Chlorophyll specific growth rate (d⁻¹) for Prochlorococcus marinus MIT9313 (Low-*
552 *Light (LLIV) deep ocean clade) vs. photoperiod (h). Rows separate data from levels of*
553 *imposed dissolved O₂ concentrations (250 µM, 25 µM and 2.5 µM). Columns separate data from*
554 *3 levels of peak imposed Photosynthetically Active Radiation (PAR; 30, 90 and 180 µmol*
555 *photons m⁻² s⁻¹). Colours represent the imposed spectral waveband (nm). Large circles show*
556 *mean or single determinations of growth rate from logistic curve fits; small circles show values*
557 *for replicate determinations, if any: replicates often fall with larger circles.*

558

559 The GAM model in Fig. 8 summarizes MIT9313 growth responses to red (A-C) or blue
560 (D-F) peak PAR and photoperiod. Under 250 $\mu\text{M O}_2$, Fig. 8D shows MIT9313 achieves fastest
561 growth rates between blue peak PAR of 30 $\mu\text{mol photons m}^{-2} \text{s}^{-1}$ and 50 $\mu\text{mol photons m}^{-2} \text{s}^{-1}$
562 ¹ and photoperiods longer than 12 h, indicated by the contour line labeled 0.52 d^{-1}
563 representing the 90th percentile of achieved growth rates. Fig. 8D also shows that growth
564 rate increases with longer photoperiods, as long as the blue peak PAR levels remain below
565 50 $\mu\text{mol photons m}^{-2} \text{s}^{-1}$. In contrast, under red light and 250 $\mu\text{M O}_2$ MIT9313 grows faster
566 while exploiting higher peak PAR and longer photoperiods. Fig. 8E shows that MIT9313 can
567 exploit all blue PAR levels and most photoperiods with 90th percentile of fastest growth rate
568 between 30 to 100 $\mu\text{mol photons m}^{-2} \text{s}^{-1}$ PAR. Fig. 8F shows that MIT9313 maintains growth
569 even under 2.5 $\mu\text{M O}_2$, under photoperiods between 8 and 12 h and peak blue PAR between
570 50 to 100 $\mu\text{mol photons m}^{-2} \text{s}^{-1}$ PAR. Thus the designation of MIT9313 as a LL clade is
571 dependent upon $[\text{O}_2]$ and light spectra (Fig. 8E).

572

573

574 *Fig. 8: Contour plot of a Generalized Additive Model (GAM) representing the chlorophyll*
575 *specific growth rate (d^{-1}) for Prochlorococcus marinus MIT9313 grown under 660 nm*
576 *(red) or 450 nm (blue) light. X-axis is photoperiod (h). Y-axis is Photosynthetically Active*
577 *Radiation (PAR; $\mu\text{mol photons m}^{-2} \text{s}^{-1}$). A. represents the model under 250 μM of O_2 and red*
578 *light. B. represents the model under 25 μM of O_2 and red light. C. represents the model under*
579 *2.5 μM of O_2 and red light. D. represents the model under 250 μM of O_2 and blue light. E.*
580 *represents the model under 25 μM of O_2 and blue light. F. represents the model under 2.5 μM of*
581 *O_2 and blue light. Legends represent a colour gradient of growth rate from no growth (white)*
582 *to 1.00 d^{-1} (dark red or dark blue). Labeled contour lines indicate the 90%, 50%, and 10%*
583 *quantiles for achieved growth rate.*

584

585 **PUR and growth responses**

586 Cumulative diel PUR can potentially collapse photoperiod, PAR and spectral
587 wavebands to a common metric of usable photosynthetically active light per day. Cumulative
588 diel PUR ($\mu\text{mol photons m}^{-2} \text{ d}^{-1}$) was calculated from PUR ($\mu\text{mol photons m}^{-2} \text{ s}^{-1}$) and
589 photoperiod (h) (Equation (4)). We plotted growth rates vs. cumulative diel PUR to
590 determine whether growth is a simple response to diel PUR, across imposed spectral
591 wavebands, and photoperiods, or whether spectral wavebands or photoperiods have
592 specific or interactive influences on growth, beyond cumulative diel PUR.

593 Due to the absorption of *P. marinus* pigments in the blue spectral waveband range,
594 the maximum cumulative diel PUR under blue light is almost 3 times that of white LED light,
595 and about 5 times that of the red light (Fig. 1), despite being derived from the same
596 photoperiods and peak PAR regimes. As such, only blue light experiments extend beyond a
597 cumulative diel PUR of $\sim 2 \times 10^6 \mu\text{mol photons m}^{-2} \text{ d}^{-1}$. This spectral bias in the range of PUR
598 leads us to caution in comparing model fits of growth in response to cumulative diel PUR
599 under red vs. blue wavebands. Furthermore, we found some distinct model fits for specific
600 photoperiods, contributing to scatter within the red vs. blue data sets.

601 The representative of HLI clade, *P. marinus* MED4, showed no growth under any 4 h
602 photoperiod treatments, even when a 4 h photoperiod delivered cumulative diel PUR
603 equivalent to other photoperiod treatments (S4 Fig.A-C). In parallel MED4 showed no
604 growth under 2.5 $\mu\text{M O}_2$, no matter the level of diel cumulative PUR. In contrast, under 250
605 or 25 $\mu\text{M O}_2$, and including photoperiods greater than 4 h, MED4 growth under blue light was
606 described by a saturating response of growth [53] to increasing cumulative diel PUR, with

607 saturation of growth rate achieved around 1.0×10^6 $\mu\text{mol m}^{-2}\text{d}^{-1}$ (Fig. 9A and B), and no
608 evidence of inhibition of growth at any achieved cumulative diel PUR. Under the ‘artificial’
609 growth treatment of red light, MED4 achieved more growth per unit diel cumulative PUR
610 (Fig. 9A and B), consistent with Murphy *et al.* [59], who showed a lower cost for growth
611 under red light, for MED4, because red light provokes less photoinactivation of PSII, than
612 equivalent levels of blue light. For distinct fits for different photoperiods refer to S4 Fig. A-C.

613 The representative of the LLII/III clade, *P. marinus* SS120 showed almost no growth
614 under 2.5 $\mu\text{M O}_2$ experiments (S4 Fig.F). Most 4 h photoperiod treatments of SS120 also did
615 not grow under 250 $\mu\text{M O}_2$, even when a 4 h photoperiod delivered cumulative diel PUR
616 equivalent to other photoperiod treatments (S4 Fig.D). Again using [53], SS120 did not grow
617 when exposed to more than $\sim 1.0 \times 10^6$ $\mu\text{mol photons m}^{-2} \text{d}^{-1}$ of cumulative diel PUR under
618 any spectral waveband or photoperiod combination, under 250 $\mu\text{M O}_2$ (S4 Fig.D).

619 Under both 25 and 250 $\mu\text{M O}_2$ experiments, SS120 growth plateaued by about $5.0 \times$
620 10^5 $\mu\text{mol photons m}^{-2} \text{d}^{-1}$ diel PUR, with some scatter among photoperiod and spectral
621 waveband regimes. The onset of growth inhibition extended to higher cumulative diel PUR
622 for cultures under 25 $\mu\text{M O}_2$, showing that SS120 is partially protected from photoinhibition
623 of growth by 25 $\mu\text{M O}_2$. Under 25 $\mu\text{M O}_2$, red light again generated more growth of SS120 per
624 unit cumulative diel PUR, than did blue light, consistent with lower cost of growth through
625 lower photoinactivation under red light (Fig. 9E) [59]. For distinct fits for different
626 photoperiods refer to S4 Fig. D-F.

627 The LLIV clade representative, *P. marinus* MIT9313, under 250 µM O₂ showed growth
628 rising to a plateau by about 5×10^5 µmol photons m⁻² d⁻¹ of cumulative diel PUR. Above about
629 1.0×10^6 µmol photons m⁻² d⁻¹ of cumulative PUR under 250 µM O₂, MIT9313 showed full
630 inhibition of growth, across photoperiods, and spectral wavebands (S4 Fig.G). Under 25 µM
631 O₂ MIT9313 showed higher growth rates over a wider plateau, with a greatly extended
632 exploitation of higher cumulative diel PUR, with full growth inhibition only above about 3.5
633 $\times 10^6$ µmol photons m⁻² d⁻¹ (S4 Fig.H). MIT9313 growth under 2.5 µM O₂ showed a wider,
634 lower, flatter response to cumulative diel PUR, with full growth inhibition only above about
635 3.5×10^6 µmol photons m⁻² d⁻¹ cumulative diel PUR (S4 Fig.I).

636 As with MED4 and SS120, our data again support enhanced growth under conditions
637 of low cumulative diel PUR and 660 nm (red) spectral bandwidth, consistent with Murphy *et*
638 *al.*[59] who found a lower cost of growth, due to decreased photoinactivation of PSII under
639 red, compared to blue, wavebands (Fig. 9G and H). Interestingly, this protective effect of red
640 light disappears for MIT9313 growing under 2.5 µM O₂, possibly because photoinactivation
641 is strongly suppressed under this low [O₂] (Fig. 9I). For distinct fits for different photoperiod
642 fits refer to S4 Fig. G-I.

643

644

645 *Fig. 9: Chlorophyll specific growth rate (d^{-1}) vs. cumulative diel Photosynthetically
646 Usable Radiation (PUR, $\mu\text{mol photons m}^{-2} d^{-1}$). Rows separate data from levels of imposed
647 dissolved O_2 concentrations as 250 μM , 25 μM and 2.5 μM . Columns separate data from strains;
648 MED4 (A-C), SS120 (D-F) and MIT9313 (G-I). Shapes show the imposed photoperiod (h); 4 h
649 (solid square), 8 h (solid diamond), 12 h (solid circle), 16 h (solid upright triangle). Symbol
650 colours show the spectral waveband for growth; 660 nm (red symbols), and 450 nm (blue
651 symbols). Large symbols show mean of growth rate from logistic curve fits; small symbols show
652 values from replicates, if any. Harrison and Platt [53] 4 parameter model fit to 660 nm (red
653 lines) or 450 nm (blue lines) growth data for each combination of strain and dissolved oxygen
654 shown with solid lines (red significantly different from blue, P value < 0.05) or dashed lines (red
655 not significantly different from blue, P value > 0.05) tested using one-way ANOVA comparisons
656 of fits.*

657

658 **Photosystem II maintenance, oxygen metabolism, and DNA repair as limitations**
659 **on *Prochlorococcus* growth**

660 Under full atmospheric [O₂] and blue light, LL clades of *Prochlorococcus* are restricted
661 to growth under low light, in part because they suffer photoinhibition of Photosystem II
662 (PSII) through several paths, including direct absorbance of UV or blue light, in parallel with
663 generation of Reactive Oxygen Species (ROS) if the electron flow is slowed [64], producing
664 damaging singlet oxygen (¹O₂) [59,64–66]. Repair of photoinactivated PSII relies on the
665 removal of damaged PsbA [67,68], followed by reassembly with newly synthesized PsbA
666 [69]. Degradation of PsbA is a rate-limiting step in recovery from photoinhibition [70],
667 mediated largely by a heterohexamer, termed in *Prochlorococcus* (FtsH1-FtsH2)₃, a
668 membrane-bound metalloprotease [71–73].

669 *Prochlorococcus* genomes encode 4 FtsH proteins [67,74], henceforth referred to as
670 FtsH1-4, homologs to the characterized FtsH isoforms of the model freshwater
671 cyanobacterium *Synechocystis* sp. PCC6803, and with presumably parallel functions (Table
672 1). Upon a shift to higher light, HLI MED4 upregulates expression of FtsH1 and FtsH2 [45],
673 homologs to the *Synechocystis* *slr0228* and *slr1604*, implicated in PSII repair [72,74]. In
674 contrast, representative LLIV strain MIT9313 shows no induction of expression of these FtsH
675 protease isoforms when shifted to high light, and thus has fewer of these FtsH hexamers
676 serving each photosystem [45]. Transcript analysis demonstrates that MIT9313 expressed
677 primarily FtsH3, homologous to *Synechocystis* *sll1463*, possibly involved in PSI biogenesis
678 [76]. FtsH3 expression did not increase in response to light stress in MIT9313 [45]. Through
679 adaptation to steady low light, clade LLIV *Prochlorococcus* instead allocate resources to
680 processes other than dynamic regulation of PSII repair.

681 *Table 1: FtsH protease homologs in Prochlorococcus marinus and the model cyanobacterium Synechocystis sp. PCC6803. Protein*
682 *homologies between Prochlorococcus and Synechocystis were determined by multiple sequence alignment with MUSCLE followed*
683 *by construction of maximum likelihood phylogenetic tree using 1000 bootstrap replicates in MEGAX.*

Organism	Homolog 1	Homolog 2	Homolog 3	Homolog 4
<i>Prochlorococcus marinus</i>	FtsH1	FtsH2	FtsH3	FtsH4
<i>Synechocystis</i> sp. PCC6803	<i>Slr0228</i>	<i>Slr1604</i>	<i>Slr1463</i>	<i>Slr1390</i>
<i>Synechocystis</i> sp. PCC6803 isoform	FtsH2	FtsH3	FtsH4	FtsH1
Function	PSII Repair	PSII Repair	PSI biogenesis	Cell viability

684

685 Ocean detections of proteins mediating protein metabolism support this
686 interpretation of distinct FtsH function across clades of *P. marinus*. Ribosome proteins from
687 clade HLI MED4, clade LLI NATL2A, clade LLII/III SS120 and clade LLIV MIT9313 show
688 generally similar patterns vs. [O₂] and depth, a proxy for peak PAR (Fig. 10). FtsH3, inferred
689 to mediate PSI assembly, likewise shows a similar pattern between MED4 and MIT9313 (Fig.
690 10). But only MED4 shows the presence of the FtsH1 & FtsH2 isoforms inferred to mediate
691 PSII repair, and then only in near-surface samples subject to higher light levels. Furthermore,
692 even though MIT9313 grows (Fig. 8), and is detected in the ocean at low [O₂] (Fig. 2), no FtsH
693 from MIT9313 is detected at low [O₂] (Fig. 10), suggesting limited requirement for protein
694 turnover under low [O₂].

695

696

697 **Fig. 10: Ocean detection of Prochlorococcus marinus protein metabolism complexes.**
698 Protein detections (circles) are plotted vs. O_2 (μM) (X-axis) and depth (m) (Y-axis) at sample
699 origin. Rows separate data annotated as from Prochlorococcus clades: HLI (including *P.*
700 *marinus* MED4, solid black circles), LLI (including *P. marinus* NATL2A, solid black circles),
701 LLII/III (including *P. marinus* SS120, solid black circles) and LLIV (including *P. marinus*
702 MIT9313, solid black circles). Columns show detections of proteins annotated as FtsH Protease
703 Complexes (FtsH1, FtsH2, FtsH3) or the Ribosome. For comparison, culture growth
704 experimental conditions are indicated by horizontal grey lines for depths approximating peak
705 Photosynthetically Active Radiation (PAR; $\mu mol\ photons\ m^{-2}\ s^{-1}$); and vertical grey lines for $[O_2]$
706 (μM). Data obtained from the Biological and Chemical Oceanography Data Management Office
707 repository [40].

708

Fig. 11 shows the measured or inferred K_M for $[O_2]$ for enzymes encoded by genes [61] from *P. marinus* strains, from clades HLI, LLI, LLII/III and LLIV. MED4 increases expression of alternative oxidase ('ubiquinol oxidase (non electrogenic)') to cope with changes in light [77], by dissipating electrons from the inter-system transport chain. The approximate K_M for $[O_2]$ of $\sim 25 \mu M$ for ubiquinol oxidase (non electrogenic) (Fig. 11) is comparable to the lower limit for growth of MED4 in our experiments (Fig. 4). We suggest that dependence upon this enzyme excludes MED4 from low oxygen zones. The genome scan shows SS120 and MIT9313 lack this gene (Fig. 11), and therefore, lack this oxygen-dependent path to cope with changing excitation. Conversely, a gene encoding (S)-2-hydroxy-acid oxidase is encoded in the MIT9313 genome (Fig. 11). (S)-2-hydroxy-acid oxidase catalyzes the reaction of 2-hydroxy acid with O_2 to produce toxic H_2O_2 [78]. (S)-2-hydroxy-acid oxidase has an approximate K_M for $[O_2]$ of $\sim 250 \mu M$, and produces H_2O_2 , so growth at lower $[O_2]$ may protect MIT9313 from auto-intoxication from production of H_2O_2 . We hypothesize that under $250 \mu M O_2$ and higher blue light, *P. marinus* MIT9313 suffered photoinhibition, resulting from the inactivation of PSII caused by the production of the reactive oxygen species, hydrogen peroxide. This photoinhibition is compounded by the limited inducible repair mechanism for PSII, due to the absence of FtsH 1 and 2 expression in *P. marinus* MIT9313 [45]. We hypothesize that under the conditions of our high light and $2.5 \mu M$ or $25 \mu M O_2$ experiments, the activity of the (S)-2-hydroxy-acid oxidase enzyme is suppressed. As a result, the catalyzed production of hydrogen peroxide is inhibited, leading to less PSII damage, allowing MIT9313 to avoid photoinhibition and circumvent its limitations on PSII repair to exploit higher light. Fig. 11 also shows that *P. marinus* SS120 is the only tested ecotype to lack the pyridoxal 5'-phosphate synthase enzyme. The pyridoxal

732 5'-phosphate synthase enzyme is an important cofactor in the biosynthesis of vitamin B₆
733 [79]. Vitamin B₆ is a potential antioxidant and can effectively quench singlet oxygen [80]. The
734 absence of the pyridoxal 5'-phosphate synthase enzyme may explain why *P. marinus* SS120
735 does not grow as well as *P. marinus* MIT9313, when exposed to high light stress under 25 μM
736 O₂ and not at all under 2.5 μM O₂ (Fig. 5).

737

738

739 **Fig. 11: K_m values for oxygen metabolizing enzymes.** The y-axis represents the log₁₀
740 concentration of oxygen substrate (μM). The x-axis represents the oxygen metabolizing
741 enzymes encoded in at least one of the *Prochlorococcus marinus* strains in this study. The
742 *Prochlorococcus marinus* strains are indicated in rows. The solid circles represent K_m values
743 from literature and the asterisks represent predicted values. colours represent the gene counts.
744 The red shaded area denotes a K_m oxygen concentration range from 230 to 280 μM . The green
745 shaded area denotes a K_m oxygen concentration range from 5 to 50 μM . The blue shaded area
746 denotes a K_m oxygen concentration range from 0.5 to 5 μM . The black bars show the minimum
747 and maximum K_m values. Figure was generated using a filtered subset of the annotated
748 phytoplankton gene sequences dataset from Omar et al. [61].

749

750 Fig. 12 shows genes encoding DNA repair for *P. marinus* strains. As expected, *P.*
751 *marinus* MED4 possesses the largest, most complete suite of genes encoding DNA repair
752 enzymes, followed by *P. marinus* MIT9313. Conversely, *P. marinus* SS120 demonstrates the
753 smallest genomic capacity for DNA repair. *Prochlorococcus marinus* MED4 and NATL2A were
754 the only strains to possess a gene encoding deoxyribodipyrimidine photolyase (Fig. 12 and
755 S5 Fig.), which, in the presence of blue light, is responsible for repairing DNA damaged by UV
756 light [81]. *Prochlorococcus marinus* MED4 was also the only strain to possess a gene
757 encoding DNA ligase, which uses ATP as a cofactor for DNA repair. The absence of genes
758 encoding deoxyribodipyrimidine photolyase and DNA ligase (ATP) in *P. marinus* MIT9313
759 and *P. marinus* SS120 explain why these two strains cannot tolerate growth under full [O₂]
760 and high light, found at the ocean surface. Furthermore, the protective effect of lower [O₂],
761 allowing these strains to grow at higher light, may relate in part to suppression of DNA
762 damage when generation of Reactive Oxygen Species is suppressed at lower [O₂]. NATL2A, a
763 clade LLI, has been found near the ocean surface during deep ocean mixing [82]. Malmstrom
764 *et al.* [82] attributes NATL2A tolerance to short exposures of high light to the presence of the
765 genes encoding photolyase, a gene found in HL clades. The presence of
766 deoxyribodipyrimidine photolyase and absence of DNA ligase (ATP) supports why NATL2A
767 tolerates limited exposure to high light and why NATL2A is unable to fully repair damaged
768 DNA. *Prochlorococcus* are highly susceptible to hydrogen peroxide (H₂O₂) toxicity as they
769 lack genes which scavenge H₂O₂ molecules [48]. The small cell size of *Prochlorococcus* allow
770 the reactive oxygen species (ROS), H₂O₂, to cross the cell membrane [83]; however,
771 accumulation of extracellular H₂O₂ remains toxic to *Prochlorococcus* [48,49].

773

774 **Fig. 12: Genes encoding DNA repair enzymes.** The y-axis represents *Prochlorococcus marinus*
775 strains. The x-axis represents enzymes encoded for DNA repair found in at least one
776 *Prochlorococcus marinus* strain in this study. Point size indicate gene counts. Figure was
777 generated using a filtered subset of the annotated phytoplankton gene sequences dataset from
778 Omar et al. [61].

779

780 The potential for niche expansion into temperate regions by *P. marinus* varies
781 depending on the season, which influences achieved underwater photoperiods and light
782 levels. Temperate summer delivers 11 hours of blue waveband light underwater, above the
783 photic threshold of 20 $\mu\text{mol photons m}^{-2} \text{s}^{-1}$, while temperate spring/fall delivers 8 hours of
784 blue waveband light underwater, photoperiod ranges which are permissive for growth of all
785 three *P. marinus*. In contrast temperate winter delivers only about 2 h of blue waveband light
786 underwater above the photic threshold, which precludes growth of MED4 and SS120, even
787 if winter waters reached permissive temperatures. MIT9313 and SS120 will be excluded
788 from near-surface growth niches by high PAR, unless OMZ zones extend to the near surface.

789 Diverse *P. marinus* strains [5] differentially exploit potential photoregimes, both at
790 the surface and deep in the water column. Some *P. marinus* strains grow under low oxygen
791 environments, similar to OMZ. The LL clades we tested can function as 'HL' in oxygen
792 environments of 25 μM , and as low as 2.5 μM , in the case of MIT9313.

793 West *et al.* [19] and Malmstrom *et al.* [82] found that decreased abundances of the LL
794 clades corresponded to increased depth of the surface mixed layer. Malmstrom *et al.* [82]
795 attributes the transport of LL ecotypes to the surface and consequent exposure to
796 photoinhibitory high light levels as the reason for low cell abundances with increased mixed
797 layer depth. West *et al.* [19] found the depth of the mixed layer strongly influenced the depth
798 transition from HL to LL clades, but that factors other than light levels may influence the
799 variations in the upper and lower depth limits of these ecotypes. We hypothesize that low
800 cell abundances of LL ecotypes in the mixed layer is likely driven in part by increased $[O_2]$,
801 and it is $[O_2]$ that constrains LL clades to deeper waters, not necessarily the light level. We

802 found that under 25 μM O_2 representatives of 'LL' clades, SS120 and MIT9313, actually
803 tolerate approximately $1.0 \times 10^6 \mu\text{mol photons m}^{-2} \text{ d}^{-1}$ of PUR (S4 Fig.E and H), comparable
804 to the representative HL clade, MED4 which also exhibited growth saturation at the same
805 cumulative diel PUR of $1.0 \times 10^6 \mu\text{mol photons m}^{-2} \text{ d}^{-1}$ (S4 Fig.A and B). Growth under lower
806 O_2 allowed MIT9313 to substantially increase its exploitation of higher diel PUR (S4 Fig.I).

807 **Summary and conclusions**

808 We analyzed growth rates for *P. marinus* clade HLI found near the ocean surface; clade
809 LLII/III found deep in the water column; and clade LLIV also found in deep oceans, including
810 OMZ, under a matrix of spectral wavebands, irradiances, photoperiods and oxygen
811 concentrations approximating present day and hypothetical future niches.

812 *Prochlorococcus marinus* MED4 requires more than 4 h of light per day; thus this
813 strain will not exploit habitats typical of temperate winter or light attenuated depths, even if
814 water temperatures warm into the clade HLI tolerance range. MED4 is also excluded from
815 the lowest oxygen habitats of 2.5 μM O_2 , but can, grow under OMZ regions with 25 μM O_2 .
816 Genomic (Fig. 11) and transcriptional analyses [77] suggest MED4 is excluded from growth
817 below $\sim 25 \mu\text{M}$ O_2 because it relies upon a ubiquinol oxidase, non-electrogenic, to maintain
818 oxidation/reduction balance in the intersystem electron transport chain, with a K_M for $[\text{O}_2]$
819 of $\sim 25 \mu\text{M}$ O_2 . On the other hand, MED4 shows inducible expression of FtsH isoforms [45],
820 to counter photoinactivation of PSII under higher PAR and $[\text{O}_2]$ environments. However,
821 photoinactivation imposes an increased cost of growth upon MED4, since growth under red
822 light, to lower photoinactivation of PSII [59], allows MED4 to achieve faster growth per

823 absorbed photon than growth under blue light. TARA Oceans Project data [20] indeed
824 reported presence of *P. marinus* MED4-like genomes at depths ranging from 5 m to 90 m,
825 representing high to low blue light levels, in the Pacific South East Ocean. Delmont and Eren
826 [20] did not analyze data from depths beyond the subsurface chlorophyll maximum layer,
827 nor did they report [O_2] at depth. Our growth findings are consistent with Fig. 2 showing PSII
828 proteins annotated as MED4, clade HLI, at depths up to 200 meters, with O_2 of ~15 μM .

829 *Prochlorococcus marinus* SS120, a LLII/III clade representative, showed an
830 interactive inhibition of growth by oxygen and cumulative diel PUR, with a higher tolerance
831 for higher cumulative diel PUR under 25 μM O_2 , compared to 250 μM O_2 (S4 Fig.). Thus, SS120
832 can exploit higher PAR environments, within OMZ. SS120 is likely excluded from the
833 combination of higher [O_2] and higher PAR by genomic limitations on capacity for DNA repair
834 (Fig. 12), and possibly by limited capacity for synthesis of reactive oxygen quenchers (Fig.
835 11). Our growth results are supported by Lavin *et al.* [10] who found evidence of LLII/III and
836 LLIV ecotypes, using terminal restriction fragment length polymorphism analyses, at depths
837 above 40 m, where light levels are higher, within OMZ, and by Fig. 2 showing PSII protein
838 subunits annotated as derived from SS120 at all depths ranging from 20 to 200 m and all [O_2]
839 in an OMZ of the tropical North Pacific Ocean. SS120 grew under photoperiods longer than 4
840 h and showed increasing growth rate with increasing photoperiods, and so has the potential
841 to thrive in deep temperate zones, specifically during the spring, summer, and fall seasons
842 when the duration of daylight exceeds 4 h, if [O_2] are near surface saturation of about 250
843 μM . Under lower oxygen levels of 25 μM , SS120 can also potentially exploit a 4 h photoperiod

844 in the blue waveband, and thus has the potential to inhabit a potential warmed, deep,
845 temperate OMZ, during the winter season.

846 *Prochlorococcus marinus* MIT9313, a LLIV clade representative, shows potential to
847 inhabit future warmer temperate zones year-round, as it grows under a 4 h photoperiod,
848 expected in winter, or at light-attenuated depths. MIT9313 demonstrates an unexpected
849 tolerance to higher light levels and cumulative diel PUR, but only under low oxygen
850 conditions of 25 μM and 2.5 μM (Fig. 7), enabling MIT9313 to grow in OMZ, even at depths
851 closer to the surface. MIT9313 carries a gene encoding (S)-2-hydroxy-acid oxidase [78], with
852 a K_M for $[\text{O}_2]$ of $\sim 250 \mu\text{M}$ (Fig. 11), which produces H_2O_2 . Growth at lower $[\text{O}_2]$ may protect
853 MIT9313 from auto-intoxication from production of H_2O_2 . We hypothesize that under 250
854 μM O_2 and higher blue light, *P. marinus* MIT9313 suffers photoinhibition, resulting in part
855 from the inactivation of PSII caused by the production of H_2O_2 . This photoinhibition is
856 compounded by limited inducible repair for PSII, due to the absence of FtsH 1 and 2
857 expression in *P. marinus* MIT9313 [45]. MIT9313 shows remarkable ability to thrive under
858 very low $[\text{O}_2]$, potentially allowing it to expand into broader ecological niches. These results
859 are supported by Fig. 2 showing PSI protein subunits annotated as derived from MIT9313
860 detected at depths $> 120 \text{ m}$, along with PSII subunits at depths from 50 m to 200 m in regions
861 where O_2 was 15 μM . Bagby and Chisholm [84] suggest that O_2 has a protective role in
862 *Prochlorococcus* under lower carbon dioxide environments when carbon fixation is limited.
863 The deep water environments typical for MIT9313 are relatively nutrient rich, and
864 *Prochlorococcus* take up and metabolize various sugars [85–87] and amino acids [88]. In
865 future work we aim to test whether MIT9313 is using photosynthesis to drive CO_2 fixation

866 in low O₂ environments, or whether PSII generation of O₂ acts as an electron sink for
867 respiration, using ATP for maintenance and to take up nutrients from the surroundings.
868 Partensky *et al.* [15] indeed found that in the low-light conditions found in the OMZ, MED4,
869 SS120 and MIT9313 all became net O₂ consumers, suggesting that low light levels cause the
870 respiratory chain to consume more O₂ than the photosynthetic electron transport chain
871 generates, thus contributing to maintenance of the low O₂ environment.

872

874 **References**

- 875 1. Chisholm SW, Frankel SL, Goericke R, Olson RJ, Palenik B, Waterbury JB, et al.
876 *Prochlorococcus Marinus* nov. Gen. Nov. Sp.: An oxyphototrophic marine prokaryote
877 containing divinyl chlorophyll a and b. Archives of Microbiology. 1992;157: 297–300.
878 doi:[10.1007/BF00245165](https://doi.org/10.1007/BF00245165)
- 879 2. Partensky F, Hess WR, Vaulot D. *Prochlorococcus, a Marine Photosynthetic Prokaryote*
880 *of Global Significance*. Microbiology and Molecular Biology Reviews. 1999;63: 106–127.
- 881 3. Rocap G, Larimer FW, Lamerdin J, Malfatti S, Chain P, Ahlgren NA, et al. Genome
882 divergence in two *Prochlorococcus* ecotypes reflects oceanic niche differentiation. Nature.
883 2003;424: 1042–1047. doi:[10.1038/nature01947](https://doi.org/10.1038/nature01947)
- 884 4. Moore LR, Rocap G, Chisholm SW. Physiology and molecular phylogeny of coexisting
885 *Prochlorococcus* ecotypes. Nature. 1998;393: 464–467. doi:[10.1038/30965](https://doi.org/10.1038/30965)
- 886 5. Biller SJ, Berube PM, Lindell D, Chisholm SW. *Prochlorococcus*: The structure and
887 function of collective diversity. Nature Reviews Microbiology. 2015;13: 13–27.
888 doi:[10.1038/nrmicro3378](https://doi.org/10.1038/nrmicro3378)
- 889 6. Veldhuis M, Kraay G. Vertical distribution and pigment composition of a
890 picoplanktonic prochlorophyte in the subtropical North Atlantic:a combined study of HPLC-
891 analysis of pigments and flow cytometry. Marine Ecology Progress Series. 1990;68: 121–127.
892 doi:[10.3354/meps068121](https://doi.org/10.3354/meps068121)
- 893 7. Chisholm SW, Olson RJ, Zettler ER, Goericke R, Waterbury JB, Welschmeyer NA. A
894 novel free-living prochlorophyte abundant in the oceanic euphotic zone. Nature. 1988;334:
895 340–343. doi:[10.1038/334340a0](https://doi.org/10.1038/334340a0)
- 896 8. Partensky F, Garczarek L. *Prochlorococcus* : Advantages and Limits of Minimalism.
897 Annual Review of Marine Science. 2010;2: 305–331. doi:[10.1146/annurev-marine-120308-081034](https://doi.org/10.1146/annurev-marine-120308-081034)
- 898 9. Goericke R, Olson RJ, Shalapyonok A. A novel niche for *Prochlorococcus* Sp. In low-
900 light suboxic environments in the Arabian Sea and the Eastern Tropical North Pacific. Deep
901 Sea Research Part I: Oceanographic Research Papers. 2000;47: 1183–1205.
902 doi:[10.1016/S0967-0637\(99\)00108-9](https://doi.org/10.1016/S0967-0637(99)00108-9)
- 903 10. Lavin P, González B, Santibáñez JF, Scanlan DJ, Ulloa O. Novel lineages of
904 *Prochlorococcus* thrive within the oxygen minimum zone of the eastern tropical South
905 Pacific. Environmental Microbiology Reports. 2010;2: 728–738. doi:[10.1111/j.1758-2229.2010.00167.x](https://doi.org/10.1111/j.1758-2229.2010.00167.x)
- 906 11. Ulloa O, Henríquez-Castillo C, Ramírez-Flandes S, Plominsky AM, Murillo AA, Morgan-
907 Lang C, et al. The cyanobacterium *Prochlorococcus* has divergent light-harvesting antennae
908 and may have evolved in a low-oxygen ocean. Proceedings of the National Academy of
909 Sciences. 2021;118. doi:[10.1073/pnas.2025638118](https://doi.org/10.1073/pnas.2025638118)

- 911 12. Garcia-Robledo E, Padilla CC, Aldunate M, Stewart FJ, Ulloa O, Paulmier A, et al. Cryptic
912 oxygen cycling in anoxic marine zones. Proceedings of the National Academy of Sciences of
913 the United States of America. 2017;114: 8319–8324. doi:[10.1073/pnas.1619844114](https://doi.org/10.1073/pnas.1619844114)
- 914 13. Holtrop T, Huisman J, Stomp M, Biersteker L, Aerts J, Grébert T, et al. Vibrational
915 modes of water predict spectral niches for photosynthesis in lakes and oceans. Nature
916 Ecology & Evolution. 2021;5: 1–12. doi:[10.1038/s41559-020-01330-x](https://doi.org/10.1038/s41559-020-01330-x)
- 917 14. Johnson Z, Landry ML, Bidigare RR, Brown SL, Campbell L, Gunderson J, et al. Energetics
918 and growth kinetics of a deep *Prochlorococcus* spp. Population in the Arabian Sea.
919 Deep Sea Research Part II: Topical Studies in Oceanography. 1999;46: 1719–1743.
920 doi:[10.1016/S0967-0645\(99\)00041-7](https://doi.org/10.1016/S0967-0645(99)00041-7)
- 921 15. Partensky F, Mella-Flores D, Six C, Garczarek L, Czjzek M, Marie D, et al. Comparison
922 of photosynthetic performances of marine picocyanobacteria with different configurations
923 of the oxygen-evolving complex. Photosynthesis Research. 2018. doi:[10.1007/s11120-018-0539-3](https://doi.org/10.1007/s11120-018-0539-3)
- 925 16. Johnson ZI, Zinser ER, Coe A, McNulty NP, Woodward EMS, Chisholm SW. Niche
926 Partitioning Among *Prochlorococcus* Ecotypes Along Ocean-Scale Environmental Gradients.
927 Science. 2006;311: 1737–1740. doi:[10.1126/science.1118052](https://doi.org/10.1126/science.1118052)
- 928 17. Zinser ER, Johnson ZI, Coe A, Karaca E, Veneziano D, Chisholm SW. Influence of light
929 and temperature on *Prochlorococcus* ecotype distributions in the Atlantic Ocean. Limnology
930 and Oceanography. 2007;52: 2205–2220. doi:[10.4319/lo.2007.52.5.2205](https://doi.org/10.4319/lo.2007.52.5.2205)
- 931 18. Kent AG, Baer SE, Mouginot C, Huang JS, Larkin AA, Lomas MW, et al. Parallel
932 phylogeography of *Prochlorococcus* and *Synechococcus*. The ISME Journal. 2019;13: 430–
933 441. doi:[10.1038/s41396-018-0287-6](https://doi.org/10.1038/s41396-018-0287-6)
- 934 19. West NJ, Scanlan DJ. Niche-Partitioning of *Prochlorococcus* Populations in a Stratified
935 Water Column in the Eastern North Atlantic Ocean. Applied and Environmental
936 Microbiology. 1999;65: 2585–2591. doi:[10.1128/AEM.65.6.2585-2591.1999](https://doi.org/10.1128/AEM.65.6.2585-2591.1999)
- 937 20. Delmont TO, Eren AM. Linking pangenomes and metagenomes: The *Prochlorococcus*
938 metapangenome. PeerJ. 2018;6: e4320. doi:[10.7717/peerj.4320](https://doi.org/10.7717/peerj.4320)
- 939 21. Flombaum P, Gallegos JL, Gordillo RA, Rincón J, Zabala LL, Jiao N, et al. Present and
940 future global distributions of the marine Cyanobacteria *Prochlorococcus* and *Synechococcus*.
941 Proceedings of the National Academy of Sciences. 2013;110: 9824–9829.
942 doi:[10.1073/pnas.1307701110](https://doi.org/10.1073/pnas.1307701110)
- 943 22. Barton AD, Irwin AJ, Finkel ZV, Stock CA. Anthropogenic climate change drives shift
944 and shuffle in North Atlantic phytoplankton communities. Proceedings of the National
945 Academy of Sciences. 2016;113: 2964–2969. doi:[10.1073/pnas.1519080113](https://doi.org/10.1073/pnas.1519080113)
- 946 23. Li G, Talmy D, Campbell DA. Diatom growth responses to photoperiod and light are
947 predictable from diel reductant generation. Journal of Phycology. 2017;53: 95–107.
948 doi:[10.1111/jpy.12483](https://doi.org/10.1111/jpy.12483)

- 949 24. Prézelin BB. Diel periodicity in phytoplankton productivity. In: Berman T, Gons HJ,
950 Mur LR, editors. *The Daily Growth Cycle of Phytoplankton: Proceedings of the Fifth*
951 *International Workshop of the Group for Aquatic Primary Productivity (GAP)*, held at
952 Breukelen, The Netherlands 20–28 April 1990. Dordrecht: Springer Netherlands; 1992. pp.
953 1–35. doi:[10.1007/978-94-011-2805-6_1](https://doi.org/10.1007/978-94-011-2805-6_1)
- 954 25. Vaulot D, Marie D, Olson RJ, Chisholm SW. Growth of *Prochlorococcus*, a
955 Photosynthetic Prokaryote, in the Equatorial Pacific Ocean. *Science*. 1995;268: 1480–1482.
956 doi:[10.1126/science.268.5216.1480](https://doi.org/10.1126/science.268.5216.1480)
- 957 26. Garcia-Soto C, Cheng L, Caesar L, Schmidtko S, Jewett EB, Cheripka A, et al. An
958 Overview of Ocean Climate Change Indicators: Sea Surface Temperature, Ocean Heat
959 Content, Ocean pH, Dissolved Oxygen Concentration, Arctic Sea Ice Extent, Thickness and
960 Volume, Sea Level and Strength of the AMOC (Atlantic Meridional Overturning Circulation).
961 *Frontiers in Marine Science*. 2021;8. doi:[10.3389/fmars.2021.642372](https://doi.org/10.3389/fmars.2021.642372)
- 962 27. Lee CE, Downey K, Colby RS, Freire CA, Nichols S, Burgess MN, et al. Recognizing
963 Salinity Threats in the Climate Crisis. *Integrative and Comparative Biology*. 2022;62: 441–
964 460. doi:[10.1093/icb/icac069](https://doi.org/10.1093/icb/icac069)
- 965 28. Matear RJ, Hirst AC. Long-term changes in dissolved oxygen concentrations in the
966 ocean caused by protracted global warming. *Global Biogeochemical Cycles*. 2003;17.
967 doi:[10.1029/2002GB001997](https://doi.org/10.1029/2002GB001997)
- 968 29. Helm KP, Bindoff NL, Church JA. Observed decreases in oxygen content of the global
969 ocean. *Geophysical Research Letters*. 2011;38. doi:[10.1029/2011GL049513](https://doi.org/10.1029/2011GL049513)
- 970 30. Busecke JJM, Resplandy L, Ditkovsky SJ, John JG. Diverging Fates of the Pacific Ocean
971 Oxygen Minimum Zone and Its Core in a Warming World. *AGU Advances*. 2022;3:
972 e2021AV000470. doi:[10.1029/2021AV000470](https://doi.org/10.1029/2021AV000470)
- 973 31. Saito MA, Saunders JK, Chagnon M, Gaylord DA, Shepherd A, Held NA, et al.
974 Development of an Ocean Protein Portal for Interactive Discovery and Education. *Journal of*
975 *proteome research*. 2021;20: 326–336. doi:[10.1021/acs.jproteome.0c00382](https://doi.org/10.1021/acs.jproteome.0c00382)
- 976 32. Moore LR, Chisholm SW. Photophysiology of the marine cyanobacterium
977 *Prochlorococcus*: Ecotypic differences among cultured isolates. *Limnology and*
978 *Oceanography*. 1999;44: 628–638. doi:[10.4319/lo.1999.44.3.0628](https://doi.org/10.4319/lo.1999.44.3.0628)
- 979 33. Billheimer SJ, Talley LD, Martz TR. Oxygen Seasonality, Utilization Rate, and Impacts
980 of Vertical Mixing in the Eighteen Degree Water Region of the Sargasso Sea as Observed by
981 Profiling Biogeochemical Floats. *Global Biogeochemical Cycles*. 2021;35: e2020GB006824.
982 doi:[10.1029/2020GB006824](https://doi.org/10.1029/2020GB006824)
- 983 34. Morel A. Available, usable, and stored radiant energy in relation to marine
984 photosynthesis. *Deep Sea Research*. 1978;25: 673–688. doi:[10.1016/0146-6291\(78\)90623-9](https://doi.org/10.1016/0146-6291(78)90623-9)

- 986 35. Goericke R, Repeta DJ. The pigments of *Prochlorococcus Marinus*: The presence of
987 divinylchlorophyll a and b in a marine prokaryote. Limnology and Oceanography. 1992;37:
988 425–433. doi:[10.4319/lo.1992.37.2.0425](https://doi.org/10.4319/lo.1992.37.2.0425)
- 989 36. Morel A, Ahn Y-H, Partensky F, Vaulot D, Claustre H. *Prochlorococcus* and
990 *Synechococcus* : A comparative study of their optical properties in relation to their size and
991 pigmentation. Journal of Marine Research. 1993;51: 617–649.
992 doi:[10.1357/0022240933223963](https://doi.org/10.1357/0022240933223963)
- 993 37. Hess WR, Rocap G, Ting CS, Larimer F, Stilwagen S, Lamerdin J, et al. The
994 photosynthetic apparatus of *Prochlorococcus*: Insights through comparative genomics.
995 Photosynthesis Research. 2001;70: 53–71. doi:[10.1023/A:1013835924610](https://doi.org/10.1023/A:1013835924610)
- 996 38. Chang A, Jeske L, Ullrich S, Hofmann J, Koblitz J, Schomburg I, et al. BRENDA, the
997 ELIXIR core data resource in 2021: New developments and updates. Nucleic Acids Research.
998 2021;49: D498–D508. doi:[10.1093/nar/gkaa1025](https://doi.org/10.1093/nar/gkaa1025)
- 999 39. Rolling Deck To Repository. Cruise KM1128 on RV Kilo Moana. 2015.
1000 doi:[10.7284/903696](https://doi.org/10.7284/903696)
- 1001 40. Saito MA. Peptides and their spectral counts from KM1128 the METZYME expedition
1002 on R/V Kilo Moana in the tropical North Pacific in 2011. Biological and Chemical
1003 Oceanography Data Management Office (BCO-DMO); 2018.
- 1004 41. Saito MA, McIlvin MR, Moran DM, Goepfert TJ, DiTullio GR, Post AF, et al. Multiple
1005 nutrient stresses at intersecting Pacific Ocean biomes detected by protein biomarkers.
1006 Science (New York, NY). 2014;345: 1173–1177. doi:[10.1126/science.1256450](https://doi.org/10.1126/science.1256450)
- 1007 42. Saito MA, Dorsk A, Post AF, McIlvin MR, Rappé MS, DiTullio GR, et al. Needles in the
1008 blue sea: Sub-species specificity in targeted protein biomarker analyses within the vast
1009 oceanic microbial metaproteome. PROTEOMICS. 2015;15: 3521–3531.
1010 doi:[10.1002/pmic.201400630](https://doi.org/10.1002/pmic.201400630)
- 1011 43. Wickham H. Tidyverse: Easily install and load the tidyverse. 2023. Available:
1012 <https://CRAN.R-project.org/package=tidyverse>
- 1013 44. RStudio Team. RStudio: Integrated development environment for r. Boston, MA:
1014 RStudio, Inc.; 2015. Available: <http://www.posit.co/>
- 1015 45. Bonisteel EM, Turner BE, Murphy CD, Melanson J-R, Duff NM, Beardsall BD, et al.
1016 Strain specific differences in rates of Photosystem II repair in picocyanobacteria correlate to
1017 differences in FtsH protein levels and isoform expression patterns. PLOS ONE. 2018;13:
1018 e0209115. doi:[10.1371/journal.pone.0209115](https://doi.org/10.1371/journal.pone.0209115)
- 1019 46. Saunders JK, McIlvin MR, Dupont CL, Kaul D, Moran DM, Horner T, et al. Microbial
1020 functional diversity across biogeochemical provinces in the central Pacific Ocean.
1021 Proceedings of the National Academy of Sciences. 2022;119: e2200014119.
1022 doi:[10.1073/pnas.2200014119](https://doi.org/10.1073/pnas.2200014119)

- 1023 47. Saunders JK, Gaylord DA, Held NA, Symmonds N, Dupont CL, Shepherd A, et al.
1024 METATRYP v 2.0: Metaproteomic Least Common Ancestor Analysis for Taxonomic Inference
1025 Using Specialized Sequence Assemblies—Standalone Software and Web Servers for Marine
1026 Microorganisms and Coronaviruses. *Journal of Proteome Research*. 2020;19: 4718–4729.
1027 doi:[10.1021/acs.jproteome.0c00385](https://doi.org/10.1021/acs.jproteome.0c00385)
- 1028 48. Morris JJ, Kirkegaard R, Szul MJ, Johnson ZI, Zinser ER. Facilitation of Robust Growth
1029 of *Prochlorococcus* Colonies and Dilute Liquid Cultures by “Helper” Heterotrophic Bacteria.
1030 *Applied and Environmental Microbiology*. 2008;74: 4530–4534. doi:[10.1128/AEM.02479-07](https://doi.org/10.1128/AEM.02479-07)
- 1032 49. Morris JJ, Johnson ZI, Szul MJ, Keller M, Zinser ER. Dependence of the Cyanobacterium
1033 *Prochlorococcus* on Hydrogen Peroxide Scavenging Microbes for Growth at the Ocean’s
1034 Surface. *PLOS ONE*. 2011;6: e16805. doi:[10.1371/journal.pone.0016805](https://doi.org/10.1371/journal.pone.0016805)
- 1035 50. Moore LR, Goericke R, Chisholm SW. Comparative physiology of *Synechococcus* and
1036 *Prochlorococcus*: Influence of light and temperature on growth, pigments, fluorescence and
1037 absorptive properties. *Marine Ecology Progress Series*. 1995;116: 259–275. Available:
1038 <https://www.jstor.org/stable/44635011>
- 1039 51. Moore LR, Coe A, Zinser ER, Saito MA, Sullivan MB, Lindell D, et al. Culturing the
1040 marine cyanobacterium *Prochlorococcus*: *Prochlorococcus* culturing. *Limnology and
1041 Oceanography: Methods*. 2007;5: 353–362. doi:[10.4319/lom.2007.5.353](https://doi.org/10.4319/lom.2007.5.353)
- 1042 52. Berges JA, Franklin DJ, Harrison PJ. Evolution of an Artificial Seawater Medium:
1043 Improvements in Enriched Seawater, Artificial Water Over the Last Two Decades. *Journal of
1044 Phycology*. 2001;37: 1138–1145. doi:[10.1046/j.1529-8817.2001.01052.x](https://doi.org/10.1046/j.1529-8817.2001.01052.x)
- 1045 53. Harrison WG, Platt T. Photosynthesis-irradiance relationships in polar and temperate
1046 phytoplankton populations. *Polar Biology*. 1986;5: 153–164. doi:[10.1007/BF00441695](https://doi.org/10.1007/BF00441695)
- 1047 54. Zeileis A, Grothendieck G, Ryan JA. Zoo: S3 infrastructure for regular and irregular
1048 time series (z’s ordered observations). 2021. Available: <https://zoo.R-Forge.R-project.org/>
- 1049 55. Bellavia S, Gratton S, Riccietti E. A Levenberg–Marquardt method for large nonlinear
1050 least-squares problems with dynamic accuracy in functions and gradients. *Numerische
1051 Mathematik*. 2018;140: 791–825. doi:[10.1007/s00211-018-0977-z](https://doi.org/10.1007/s00211-018-0977-z)
- 1052 56. Elzhov TV, Mullen KM, Spiess A-N, Bolker B. Minpack.lm: R interface to the levenberg-
1053 marquardt nonlinear least-squares algorithm found in MINPACK, plus support for bounds.
1054 2016. Available: <https://CRAN.R-project.org/package=minpack.lm>
- 1055 57. Wood SN. Generalized Additive Models: An Introduction with R, Second Edition. 2nd
1056 ed. Boca Raton: Chapman and Hall/CRC; 2017. doi:[10.1201/9781315370279](https://doi.org/10.1201/9781315370279)
- 1057 58. Wood S. Mgc: Mixed GAM computation vehicle with automatic smoothness
1058 estimation. 2022. Available: <https://CRAN.R-project.org/package=mgc>

- 1059 59. Murphy CD, Roodvoets MS, Austen EJ, Dolan A, Barnett A, Campbell DA.
1060 Photoinactivation of Photosystem II in *Prochlorococcus* and *Synechococcus*. PLoS One; San
1061 Francisco. 2017;12: e0168991.
1062 doi:<http://dx.doi.org.libproxy.mta.ca/10.1371/journal.pone.0168991>
- 1063 60. Jávorfi T, Frostyák J, Gál J, Buzády A, Menczel L, Garab G, et al. Quantitative
1064 spectrophotometry using integrating cavities. Journal of Photochemistry and Photobiology
1065 B: Biology. 2006;82: 127–131. doi:[10.1016/j.jphotobiol.2005.10.002](https://doi.org/10.1016/j.jphotobiol.2005.10.002)
- 1066 61. Omar N, Beardsall B, Fleury K, Ataikiru E, Campbell D. Annotation of genes encoding
1067 enzymes across marine phytoplankton genomes. Dryad; 2023. pp. 1130923746 bytes.
1068 doi:[10.5061/DRYAD.KH1893284](https://doi.org/10.5061/DRYAD.KH1893284)
- 1069 62. Karp PD, Billington R, Caspi R, Fulcher CA, Latendresse M, Kothari A, et al. The BioCyc
1070 collection of microbial genomes and metabolic pathways. Briefings in Bioinformatics.
1071 2019;20: 1085–1093. doi:[10.1093/bib/bbx085](https://doi.org/10.1093/bib/bbx085)
- 1072 63. Allahverdiyeva Y, Isojärvi J, Zhang P, Aro E-M. Cyanobacterial Oxygenic
1073 Photosynthesis is Protected by Flavodiiron Proteins. Life. 2015;5: 716–743.
1074 doi:[10.3390/life5010716](https://doi.org/10.3390/life5010716)
- 1075 64. Aro E-M, Virgin I, Andersson B. Photoinhibition of Photosystem II. Inactivation,
1076 protein damage and turnover. Biochimica et Biophysica Acta (BBA) - Bioenergetics.
1077 1993;1143: 113–134. doi:[10.1016/0005-2728\(93\)90134-2](https://doi.org/10.1016/0005-2728(93)90134-2)
- 1078 65. Soitamo A, Havurinne V, Tyystjärvi E. Photoinhibition in marine picocyanobacteria.
1079 Physiologia Plantarum. 2017;161: 97–108. doi:[10.1111/ppl.12571](https://doi.org/10.1111/ppl.12571)
- 1080 66. Hakala M, Tuominen I, Keränen M, Tyystjärvi T, Tyystjärvi E. Evidence for the role of
1081 the oxygen-evolving manganese complex in photoinhibition of Photosystem II. Biochimica
1082 Et Biophysica Acta. 2005;1706: 68–80. doi:[10.1016/j.bbabi.2004.09.001](https://doi.org/10.1016/j.bbabi.2004.09.001)
- 1083 67. Mann NH, Novac N, Mullineaux CW, Newman J, Bailey S, Robinson C. Involvement of
1084 an FtsH homologue in the assembly of functional photosystem I in the cyanobacterium
1085 *Synechocystis* sp. PCC 6803. FEBS letters. 2000;479: 72–77. doi:[10.1016/s0014-5793\(00\)01871-8](https://doi.org/10.1016/s0014-5793(00)01871-8)
- 1087 68. Komenda J, Tichý M, Prášil O, Knoppová J, Kuvíková S, de Vries R, et al. The Exposed
1088 N-Terminal Tail of the D1 Subunit Is Required for Rapid D1 Degradation during Photosystem
1089 II Repair in *Synechocystis* sp PCC 6803. The Plant Cell. 2007;19: 2839–2854.
1090 doi:[10.1105/tpc.107.053868](https://doi.org/10.1105/tpc.107.053868)
- 1091 69. Nixon PJ, Michoux F, Yu J, Boehm M, Komenda J. Recent advances in understanding
1092 the assembly and repair of photosystem II. Annals of Botany. 2010;106: 1–16.
1093 doi:[10.1093/aob/mcq059](https://doi.org/10.1093/aob/mcq059)
- 1094 70. Kanervo E, Mäenpää P, Aro E-M. D1 Protein Degradation and *psbA* Transcript Levels
1095 in *Synechocystis* PCC 6803 during Photoinhibition *in Vivo*. Journal of Plant Physiology.
1096 1993;142: 669–675. doi:[10.1016/S0176-1617\(11\)80900-4](https://doi.org/10.1016/S0176-1617(11)80900-4)

- 1097 71. Chiba S, Akiyama Y, Ito K. Membrane Protein Degradation by FtsH Can Be Initiated
1098 from Either End. *Journal of Bacteriology*. 2002;184: 4775–4782.
1099 doi:[10.1128/JB.184.17.4775-4782.2002](https://doi.org/10.1128/JB.184.17.4775-4782.2002)
- 1100 72. Boehm M, Yu J, Krynicka V, Barker M, Tichy M, Komenda J, et al. Subunit Organization
1101 of a *Synechocystis* Hetero-Oligomeric Thylakoid FtsH Complex Involved in Photosystem II
1102 Repair. *The Plant Cell*. 2012;24: 3669–3683. doi:[10.1105/tpc.112.100891](https://doi.org/10.1105/tpc.112.100891)
- 1103 73. Sacharz J, Bryan SJ, Yu J, Burroughs NJ, Spence EM, Nixon PJ, et al. Sub-cellular location
1104 of Fts H proteases in the cyanobacterium *S. Ynechocystis* sp. PCC 6803 suggests localised
1105 PSII repair zones in the thylakoid membranes. *Molecular Microbiology*. 2015;96: 448–462.
1106 doi:[10.1111/mmi.12940](https://doi.org/10.1111/mmi.12940)
- 1107 74. Adam Z, Zaltsman A, Sinvany-Villalobo G, Sakamoto W. FtsH proteases in chloroplasts
1108 and cyanobacteria. *Physiologia Plantarum*. 2005;123: 386–390. doi:[10.1111/j.1399-3054.2004.00436.x](https://doi.org/10.1111/j.1399-3054.2004.00436.x)
- 1109 75. Krynická V, Skotnicová P, Jackson PJ, Barnett S, Yu J, Wysocka A, et al. FtsH4 protease
1110 controls biogenesis of the PSII complex by dual regulation of high light-inducible proteins.
1111 *Plant Communications*. 2022;4: 100502. doi:[10.1016/j.xplc.2022.100502](https://doi.org/10.1016/j.xplc.2022.100502)
- 1112 76. Koník P, Skotnicová P, Gupta S, Tichý M, Sharma S, Komenda J, et al. The
1113 cyanobacterial FtsH4 protease controls accumulation of protein factors involved in the
1114 biogenesis of photosystem I. *Biochimica et Biophysica Acta (BBA) - Bioenergetics*.
1115 2024;1865: 149017. doi:[10.1016/j.bbabi.2023.149017](https://doi.org/10.1016/j.bbabi.2023.149017)
- 1116 77. Berg G, Shrager J, Van Dijken G, Mills M, Arrigo K, Grossman A. Responses of psbA, hli
1117 and ptox genes to changes in irradiance in marine *Synechococcus* and *Prochlorococcus*.
1118 *Aquatic Microbial Ecology*. 2011;65: 1–14. doi:[10.3354/ame01528](https://doi.org/10.3354/ame01528)
- 1119 78. Cunane LM, Barton JD, Chen Z, Lê KHD, Amar D, Lederer F, et al. Crystal Structure
1120 Analysis of Recombinant Rat Kidney Long Chain Hydroxy Acid Oxidase,. *Biochemistry*.
1121 2005;44: 1521–1531. doi:[10.1021/bi048616e](https://doi.org/10.1021/bi048616e)
- 1122 79. Sang Y, Barbosa JM, Wu H, Locy RD, Singh NK. Identification of a pyridoxine
1123 (pyridoxamine) 5'-phosphate oxidase from *Arabidopsis thaliana*. *FEBS Letters*. 2007;581:
1124 344–348. doi:[10.1016/j.febslet.2006.12.028](https://doi.org/10.1016/j.febslet.2006.12.028)
- 1125 80. Bilski P, Li MY, Ehrenshaft M, Daub ME, Chignell CF. Vitamin B6 (Pyridoxine) and Its
1126 Derivatives Are Efficient Singlet Oxygen Quenchers and Potential Fungal Antioxidants.
1127 *Photochemistry and Photobiology*. 2000;71: 129–134. doi:[10.1562/0031-8655\(2000\)0710129SIPVBP2.0.CO2](https://doi.org/10.1562/0031-8655(2000)0710129SIPVBP2.0.CO2)
- 1128 81. Sancar A. Structure and Function of DNA Photolyase and Cryptochrome Blue-Light
1129 Photoreceptors. *Chemical Reviews*. 2003;103: 2203–2238. doi:[10.1021/cr0204348](https://doi.org/10.1021/cr0204348)
- 1130 82. Malmstrom RR, Coe A, Kettler GC, Martiny AC, Frias-Lopez J, Zinser ER, et al. Temporal
1131 dynamics of *Prochlorococcus* ecotypes in the Atlantic and Pacific oceans. *The ISME Journal*.
1132 2010;4: 1252–1264. doi:[10.1038/ismej.2010.60](https://doi.org/10.1038/ismej.2010.60)

- 1135 83. Omar NM, Prášil O, McCain JSP, Campbell DA. Diffusional Interactions among Marine
1136 Phytoplankton and Bacterioplankton: Modelling H₂O₂ as a Case Study. *Microorganisms*.
1137 2022;10: 821. doi:[10.3390/microorganisms10040821](https://doi.org/10.3390/microorganisms10040821)
- 1138 84. Bagby SC, Chisholm SW. Response of *Prochlorococcus* to varying CO₂:O₂ ratios. *The
1139 ISME Journal*. 2015;9: 2232–2245. doi:[10.1038/ismej.2015.36](https://doi.org/10.1038/ismej.2015.36)
- 1140 85. Gómez-Baena G, López-Lozano A, Gil-Martínez J, Lucena JM, Diez J, Candau P, et al.
1141 Glucose Uptake and Its Effect on Gene Expression in *Prochlorococcus*. *PLOS ONE*. 2008;3:
1142 e3416. doi:[10.1371/journal.pone.0003416](https://doi.org/10.1371/journal.pone.0003416)
- 1143 86. Muñoz-Marín M del C, Gómez-Baena G, Díez J, Beynon RJ, González-Ballester D,
1144 Zubkov MV, et al. Glucose Uptake in *Prochlorococcus*: Diversity of Kinetics and Effects on the
1145 Metabolism. *Frontiers in Microbiology*. 2017;8. doi:[10.3389/fmicb.2017.00327](https://doi.org/10.3389/fmicb.2017.00327)
- 1146 87. Muñoz-Marín M del C, Luque I, Zubkov MV, Hill PG, Diez J, García-Fernández JM.
1147 *Prochlorococcus* can use the Pro1404 transporter to take up glucose at nanomolar
1148 concentrations in the Atlantic Ocean. *Proceedings of the National Academy of Sciences of the
1149 United States of America*. 2013;110: 8597–8602. doi:[10.1073/pnas.1221775110](https://doi.org/10.1073/pnas.1221775110)
- 1150 88. Zubkov MV, Tarran GA, Fuchs BM. Depth related amino acid uptake by
1151 *Prochlorococcus* cyanobacteria in the Southern Atlantic tropical gyre. *FEMS Microbiology
1152 Ecology*. 2004;50: 153–161. doi:[10.1016/j.femsec.2004.06.009](https://doi.org/10.1016/j.femsec.2004.06.009)

1153

1154

1155 **Supporting information**

1156

1157 *S1 Fig.: PSI MCMIX-OD Multicultivator.* Spectral waveband, light level and photoperiod are
1158 individually controlled for each culture tube. Real time Optical Density (OD) measurements
1159 eliminate intrusive subsampling of cultures. The temperature of culture tubes are collectively
1160 controlled via heating or cooling of the aquarium water. Gas with specific oxygen
1161 concentrations is bubbled through a humidifier and passed through a 0.2 µm filter.

1162

1163

1164 **S2 Fig.: Fitting chlorophyll specific growth rate for each tube in the Multicultivator.** The
1165 x-axis is time in hours (h). The left y-axis is chlorophyll proxy optical density ($OD_{680} - OD_{720}$;
1166 ΔOD) The right y-axis is the Photosynthetically Active Radiation (PAR; $\mu\text{mol photons m}^{-2} \text{s}^{-1}$)
1167 levels; colours represent the imposed spectral waveband: 450 nm (blue points) or 660 nm (red
1168 points). The green points are ΔOD measurements taken every 5 minutes. The black lines are
1169 logistic growth curves fit using a nonlinear model regression (R package, minpack.lm). The gold
1170 points are the residuals of the fit. Meta data associated with each Multicultivator tube are in
1171 columns.

1172

1173

1174 *S3 Fig.: Normalized absorbance, emission and Photosynthetically Usable Radiation*
1175 *spectra for Prochlorococcus marinus MED4 (A-C); SS120 (D-F); MIT9313 (G-I) grown*
1176 *under three emission wavebands. (A,D,G) Growth light emission spectra from the White LED*
1177 *(normalized to 439 nm; dotted black line); whole cell absorbance spectra (normalized to*
1178 *absorbance maxima between 400 nm and 460 nm; dashed purple line); and calculated PUR*
1179 *spectra (solid black line and shaded grey). (B,E,H) Growth light emission spectra at 660 nm*
1180 *(normalized to 647 nm; dotted red line); whole cell absorbance spectra (normalized to*
1181 *absorbance maxima between 400 nm and 460 nm; dashed purple line); and calculated PUR*
1182 *spectra (solid black line and shaded red). (C,F,I) Growth light emission spectra at 450 nm*
1183 *(normalized to 441 nm; dotted blue line); whole cell absorbance spectra (normalized to*
1184 *absorbance maxima between 400 nm and 460 nm; dashed purple line); and calculated PUR*
1185 *spectra (solid black line and shaded blue). Photosynthetically Active Radiation (PAR; μmol*
1186 *photons $\text{m}^{-2} \text{s}^{-1}$) and calculated Photosynthetically Usable Radiation (PUR; $\mu\text{mol photons m}^{-2} \text{s}^{-1}$)*
1187 *levels are indicated.*

1188

1189

1190 *S4 Fig.: Chlorophyll specific growth rate (d^{-1}) vs. cumulative diel Photosynthetically
1191 Usable Radiation (PUR, $\mu\text{mol photons m}^{-2} d^{-1}$).* Rows separate data from levels of imposed
1192 dissolved O_2 concentrations as 250 μM , 25 μM and 2.5 μM . Columns separate data from strains;
1193 MED4 (A-C), SS120 (D-F) and MIT9313 (G-I). Shapes show the imposed photoperiod (h); 4 h
1194 (solid square), 8 h (solid diamond), 12 h (solid circle), 16 h (solid upright triangle). Symbol
1195 colours show the spectral waveband for growth; white LED (black symbols), 660 nm (red
1196 symbols), and 450 nm (blue symbols). Large symbols show mean of growth rate from logistic
1197 curve fits; small symbols show values for replicate determinations, if any. Harrison and Platt
1198 [53] 4 parameter model fit to data pooled for each combination of strain and dissolved oxygen
1199 shown with solid lines. Separate models fit to photoperiod data and shown if significantly
1200 different (P value < 0.05) from the pooled model using one-way ANOVA; 4 h (long dashed line);
1201 8 h (dotted line); 12 h (dashed line); and 16 h (dot dashed line).

1202

1203

1204 **S5 Fig.: Prochlorococcus genes encoding enzymes activated or inhibited by light.** The y-
1205 axis represents *Prochlorococcus marinus* strains. The x-axis represents enzymes encoding light-
1206 dependent enzymes found in at least one *Prochlorococcus marinus* strain in this study. Point
1207 size indicate gene counts. Figure was generated using a filtered subset of the annotated
1208 phytoplankton gene sequences dataset from Omar et al. [61].

1209

1210 S1 Table: Enzymes shown in Figures 11, 12 and 17 with their Enzyme Commission numbers
 1211 (EC) and Kegg Orthology (KO).

Enzyme Name	EC	Kegg Orthology
quinate dehydrogenase	1.1.1.24	K09484
pyranose oxidase	1.1.3.10	K23272
L-sorbose oxidase	1.1.3.11	NA
pyridoxine 4-oxidase	1.1.3.12	K18607
alcohol oxidase	1.1.3.13	K17066
(S)-2-hydroxy-acid oxidase	1.1.3.15	K00104
(S)-2-hydroxy-acid oxidase	1.1.3.15	K11517
ecdysone oxidase	1.1.3.16	K10724
choline oxidase	1.1.3.17	K17755
secondary-alcohol oxidase	1.1.3.18	NA
4-hydroxymandelate oxidase (decarboxylating)	1.1.3.19	NA
long-chain-alcohol oxidase	1.1.3.20	K17756
long-chain-alcohol oxidase	1.1.3.20	NA
glycerol-3-phosphate oxidase	1.1.3.21	K00105
thiamine oxidase	1.1.3.23	NA
hydroxyphytanate oxidase	1.1.3.27	NA
nucleoside oxidase	1.1.3.28	NA
polyvinyl-alcohol oxidase	1.1.3.30	NA
D-arabinono-1,4-lactone oxidase	1.1.3.37	K00107
vanillyl-alcohol oxidase	1.1.3.38	K20153
nucleoside oxidase (H ₂ O ₂ -forming)	1.1.3.39	NA
glucose oxidase	1.1.3.4	NA
D-mannitol oxidase	1.1.3.40	NA
alditol oxidase	1.1.3.41	K00594
prosolanapyrone-II oxidase	1.1.3.42	K20550
aclacinomycin-N oxidase	1.1.3.45	K15949
4-hydroxymandelate oxidase	1.1.3.46	K16422
5-(hydroxymethyl)furfural oxidase	1.1.3.47	K16873
3-deoxy-alpha-D-manno-octulosonate 8-oxidase	1.1.3.48	K19714
hexose oxidase	1.1.3.5	K21840
cholesterol oxidase	1.1.3.6	K03333
aryl-alcohol oxidase	1.1.3.7	NA
L-gulonolactone oxidase	1.1.3.8	K00103
galactose oxidase	1.1.3.9	K04618
glycerol oxidase	1.1.3.B4	NA
(S)-2-hydroxyglutarate dehydrogenase	1.1.5.13	NA
decaprenylphospho-beta-D-ribofuranose dehydrogenase	2-	1.1.98.3
cellobiose dehydrogenase (acceptor)		1.1.99.18
		NA

Enzyme Name	EC	Kegg Orthology
glucooligosaccharide oxidase	1.1.99.B3	NA
catechol oxidase	1.10.3.1	K00422
ubiquinol oxidase (non-electrogenic)	1.10.3.11	K17893
grixazone synthase	1.10.3.15	K20204
superoxide oxidase	1.10.3.17	K12262
laccase	1.10.3.2	K00421
laccase	1.10.3.2	K05909
L-ascorbate oxidase	1.10.3.3	K00423
L-ascorbate oxidase	1.10.3.3	NA
o-aminophenol oxidase	1.10.3.4	K20204
o-aminophenol oxidase	1.10.3.4	K20219
3-hydroxyanthranilate oxidase	1.10.3.5	NA
rifamycin-B oxidase	1.10.3.6	NA
catechol 1,2-dioxygenase	1.13.11.1	K03381
7,8-dihydroxykynurenate 8,8a-dioxygenase	1.13.11.10	NA
tryptophan 2,3-dioxygenase	1.13.11.11	K00453
linoleate 13S-lipoxygenase	1.13.11.12	K00454
2,3-dihydroxybenzoate 3,4-dioxygenase	1.13.11.14	K10621
3,4-dihydroxyphenylacetate 2,3-dioxygenase	1.13.11.15	K00455
3-carboxyethylcatechol 2,3-dioxygenase	1.13.11.16	K05713
indole 2,3-dioxygenase	1.13.11.17	NA
persulfide dioxygenase;	1.13.11.18	K17725
cysteamine dioxygenase	1.13.11.19	K10712
catechol 2,3-dioxygenase	1.13.11.2	K00446
catechol 2,3-dioxygenase	1.13.11.2	K07104
4-hydroxyphenylpyruvate dioxygenase	1.13.11.27	K00457
protocatechuate 3,4-dioxygenase	1.13.11.3	K00448
protocatechuate 3,4-dioxygenase	1.13.11.3	K00449
arachidonate 15-lipoxygenase	1.13.11.33	K00460
arachidonate 15-lipoxygenase	1.13.11.33	K08022
arachidonate 15-lipoxygenase	1.13.11.33	K19246
arachidonate 5-lipoxygenase	1.13.11.34	K00461
acireductone dioxygenase (Ni ²⁺ -requiring)	1.13.11.53	K08967
linolenate 9R-lipoxygenase	1.13.11.61	K18031
all-trans-8'-apo-beta-carotenal 15,15'-oxygenase	1.13.11.75	K00464
7,8-dihydronopterin oxygenase	1.13.11.81	K01633
peptide-aspartate beta-dioxygenase	1.14.11.16	K00476
taurine dioxygenase	1.14.11.17	K03119
procollagen-proline 4-dioxygenase	1.14.11.2	K00472
nitric oxide dioxygenase	1.14.12.17	K05916
salicylate 1-monooxygenase	1.14.13.1	K00480

Enzyme Name	EC	Kegg Orthology
cyclohexanone monooxygenase	1.14.13.22	K03379
violacein synthase	1.14.13.224	K20090
L-lysine N6-monooxygenase (NADPH)	1.14.13.59	K03897
magnesium-protoporphyrin IX monomethyl ester (oxidative) cyclase	1.14.13.81	K04035
kynurenine 3-monooxygenase	1.14.13.9	K00486
unspecific monooxygenase	1.14.14.1	K00490
dimethylsulfone monooxygenase	1.14.14.35	K17228
heme oxygenase (biliverdin-producing, ferredoxin)	1.14.15.20	K21480
choline monooxygenase	1.14.15.7	K00499
stearoyl-CoA 9-desaturase	1.14.19.1	K00507
acyl-lipid (n+3)-(Z)-desaturase (ferredoxin)	1.14.19.23	K10255
tetracycline 7-halogenase	1.14.19.49	K14257
tryptophan 7-halogenase	1.14.19.9	K14266
ferroxidase	1.16.3.1	NA
bacterial non-heme ferritin	1.16.3.2	NA
xanthine dehydrogenase	1.17.1.4	NA
(light-dependent) protochlorophyllide reductase	1.3.1.33	NA
coproporphyrinogen oxidase	1.3.3.3	NA
9,9'-dicis-zeta-carotene desaturase	1.3.5.6	NA
short-chain acyl-CoA dehydrogenase	1.3.8.1	NA
dihydroorotate dehydrogenase (fumarate)	1.3.98.1	NA
L-aspartate oxidase	1.4.3.16	NA
glycine oxidase	1.4.3.19	NA
D-amino-acid oxidase	1.4.3.3	NA
monoamine oxidase	1.4.3.4	NA
pyridoxal 5'-phosphate synthase	1.4.3.5	NA
nitrate reductase (NADH)	1.7.1.1	NA
ferredoxin-nitrate reductase	1.7.7.2	NA
cytochrome-c oxidase	1.9.3.1	NA
thymidylate synthase (FAD)	2.1.1.148	NA
5-aminolevulinate synthase	2.3.1.37	NA
aralkylamine N-acetyltransferase	2.3.1.87	NA
sucrose-phosphate synthase	2.4.1.14	NA
protein O-GlcNAc transferase	2.4.1.255	NA
15-cis-phytoene synthase	2.5.1.32	NA
4-(cytidine 5'-diphospho)-2-C-methyl-D-erythritol kinase	2.7.1.148	NA
crossover junction endodeoxyribonuclease	3.1.22.4	NA
3',5'-cyclic-GMP phosphodiesterase	3.1.4.35	NA
phospholipase D	3.1.4.4	NA

Enzyme Name	EC	Kegg Orthology
DNA-3-methyladenine glycosylase II	3.2.2.21	NA
leucyl aminopeptidase	3.4.11.1	NA
glutamyl endopeptidase	3.4.21.19	NA
ribulose-bisphosphate carboxylase	4.1.1.39	NA
deoxyribodipyrimidine photo-lyase	4.1.99.3	NA
deoxyribodipyrimidine photo-lyase	4.1.99.3	NA
aldehyde oxygenase (deformylating)	4.1.99.5	NA
nitrile hydratase	4.2.1.84	NA
chorismate synthase	4.2.3.5	NA
DNA-(apurinic or apyrimidinic site) lyase	4.2.99.18	NA
lactoylglutathione lyase	4.4.1.5	NA
adenylate cyclase	4.6.1.1	NA
guanylate cyclase	4.6.1.2	NA
long-chain-fatty-acid—CoA ligase	6.2.1.3	NA
DNA ligase (ATP)	6.5.1.1	NA
DNA ligase (NAD ⁺)	6.5.1.2	NA
cytochrome-c oxidase	7.1.1.9	NA
Flavodiiron (Flv1a/3a)	NA	NA

1213 S2 Table: The maximum growth rate, μ_{max} (d^{-1}) achieved for each strain under each $[O_2]$, with the corresponding photoperiod, PAR
 1214 level and spectral waveband.

Strain	$[O_2]$ (μM)	μ_{max} (d^{-1})	Photoperiod (h)	PAR ($\mu mol\ photons\ m^{-2}\ s^{-1}$)	Spectral waveband (nm)
MED4	250	0.68	16	180	450
MED4	25	0.65	12	90	450
MED4	2.5	0.00	All tested	All tested	All tested
SS120	250	0.50	16	90	White LED
SS120	25	0.45	8	90	450
SS120	2.5	0.15	12	30	660
MIT9313	250	0.54	16	30	450
MIT9313	25	1.01	16	90	White LED
MIT9313	2.5	0.45	12	90	450

1215

1216 **Acknowledgements**

1217 Makoto Saito for edits and feedback pertaining to the Ocean Protein Portal dataset. Miranda
1218 Corkum maintained cultures and trained personnel in culture handling. Carlie Barnhill
1219 (Mount Allison Student) assisted with code for import of multicultivator growth data files.
1220 Sarah Arthur & Daytona McMackin (Mount Allison Students) assisted with culturing and
1221 setting up Multic和平uator runs.

1222

1223

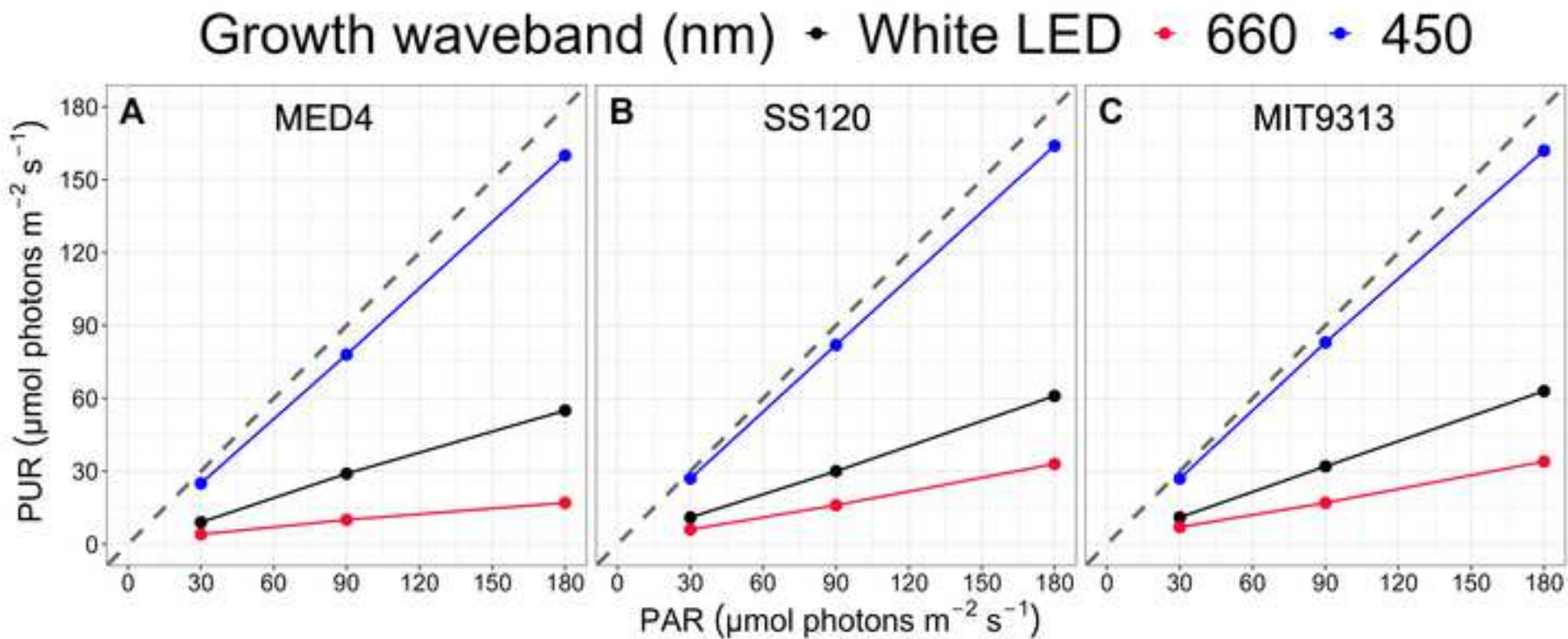


Figure 2

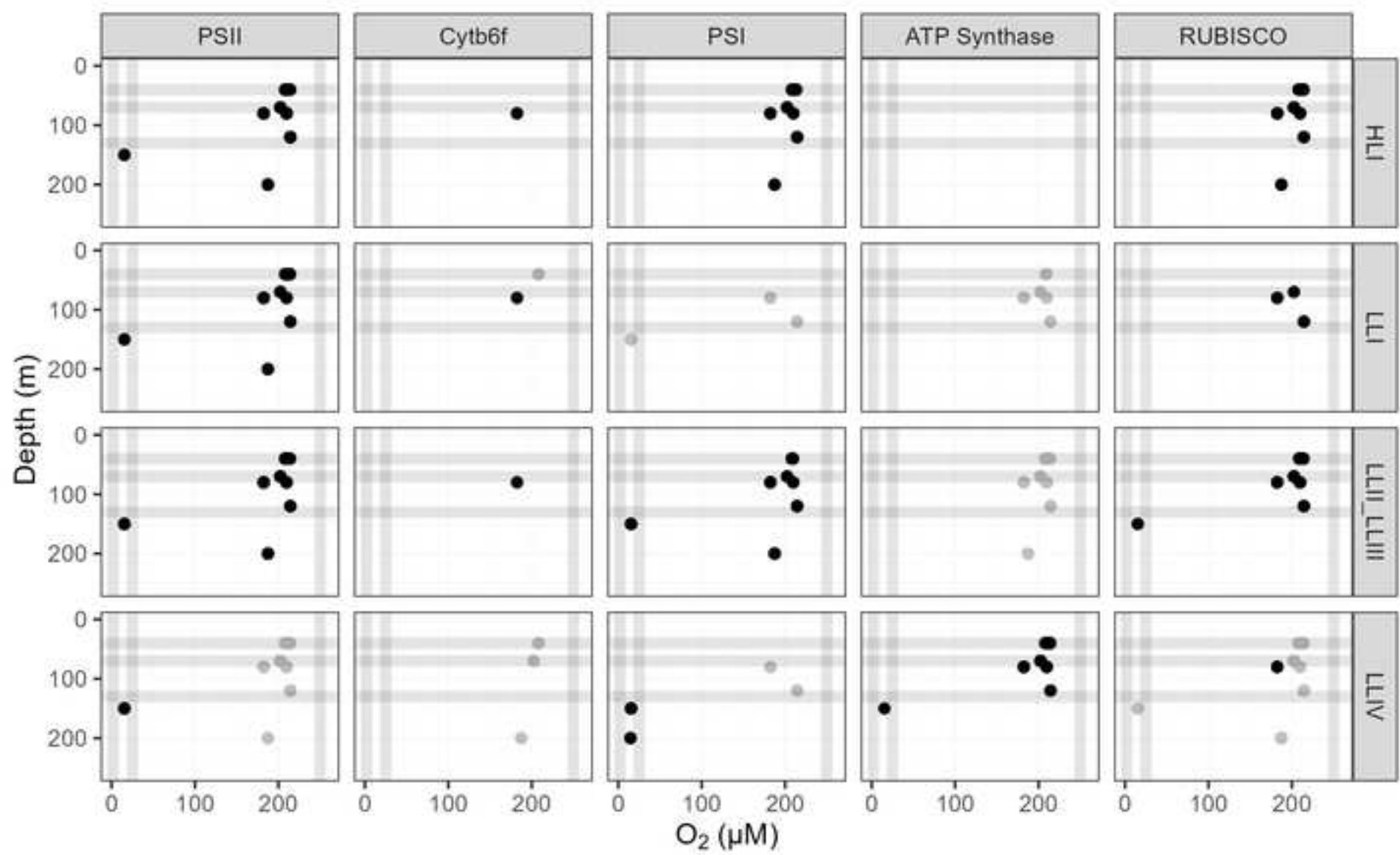
[Click here to access/download/](#)[Figure;Fig2.tiff](#)

Figure 3

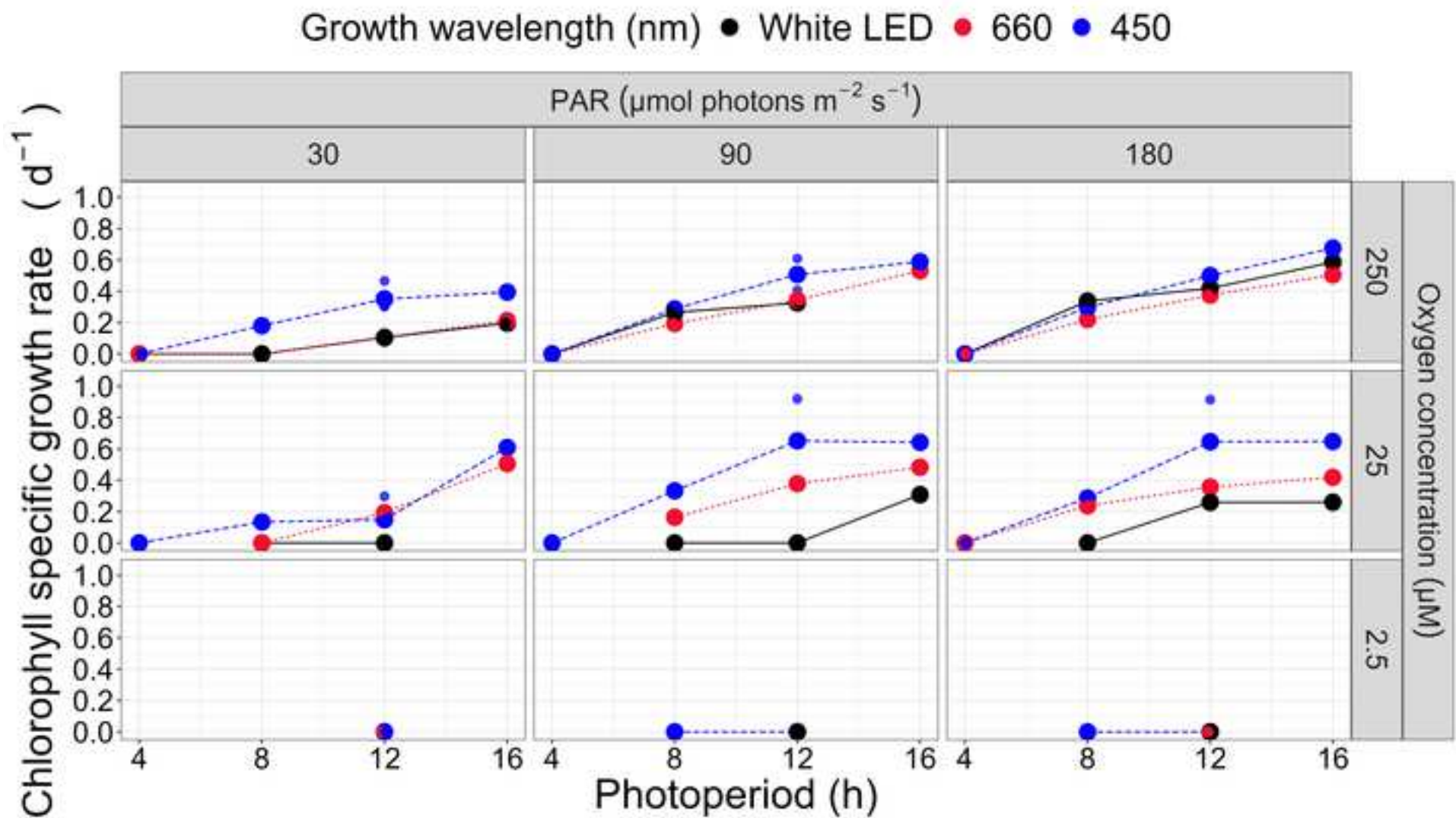
[Click here to access/download/](#)[Figure;Fig3.tif](#)

Figure 4

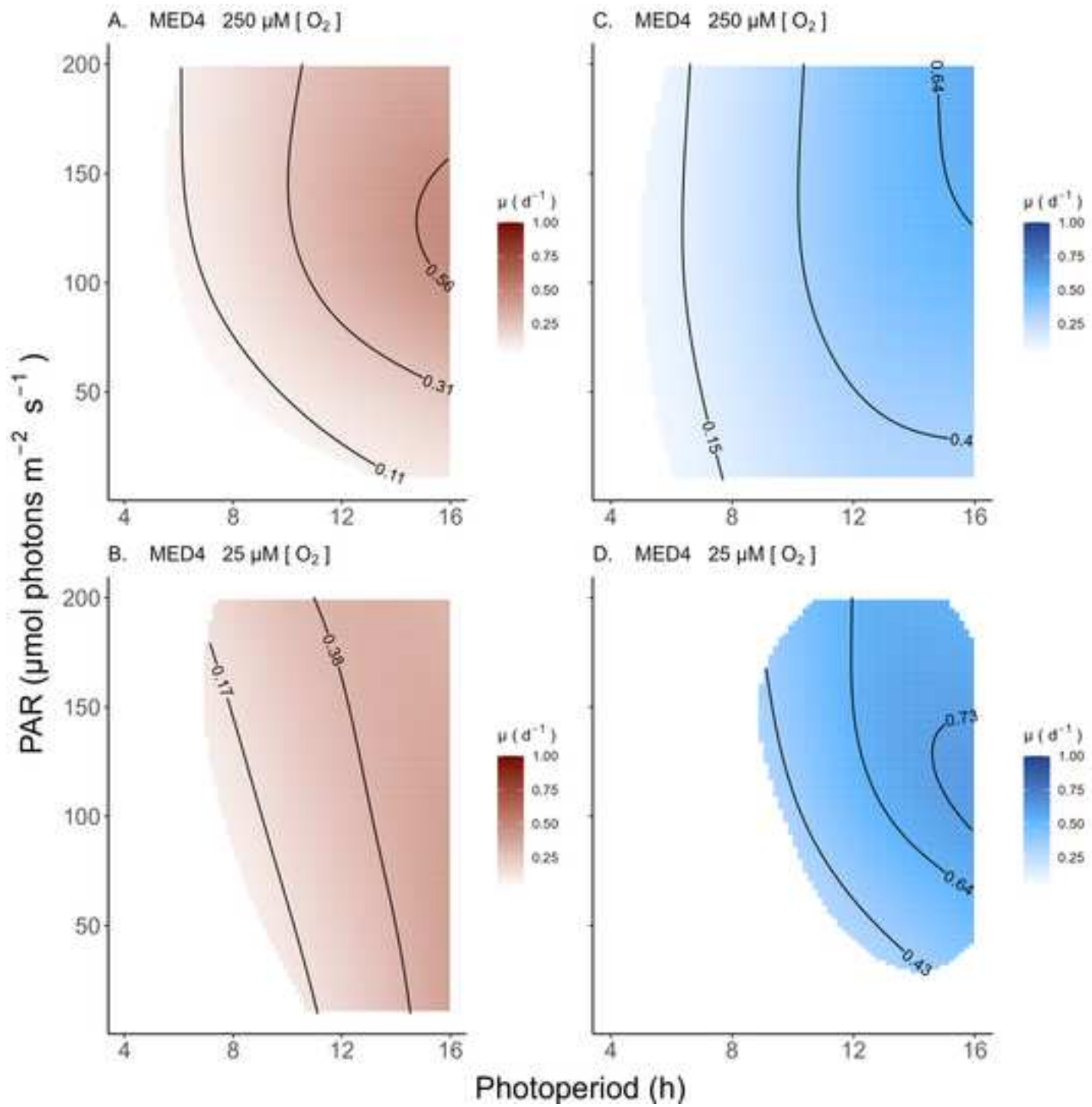
[Click here to access/download/](#)[Figure;Fig4.tif](#)

Figure 5

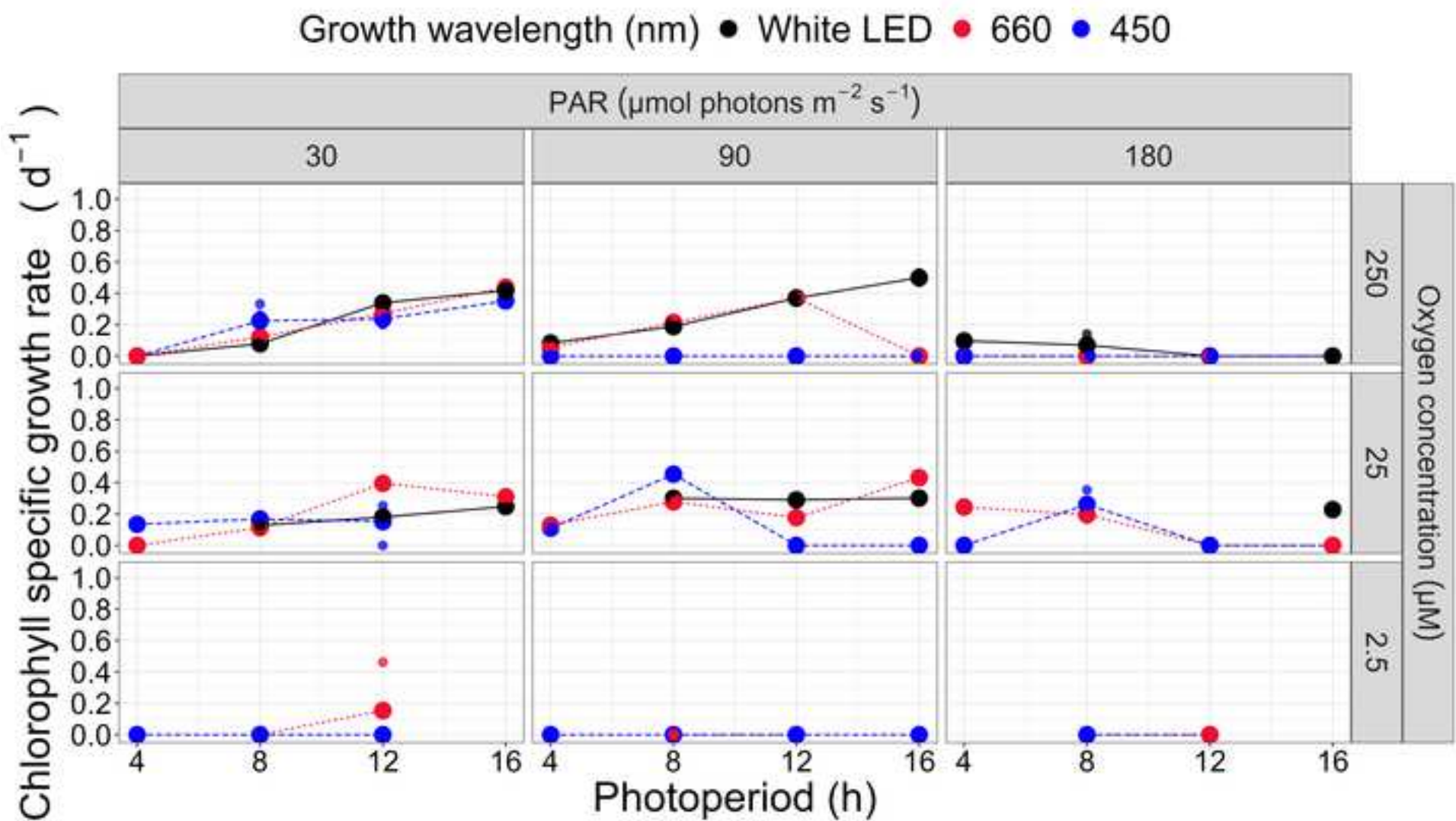
[Click here to access/download;Figure;Fig5.tif](#)

Figure 6

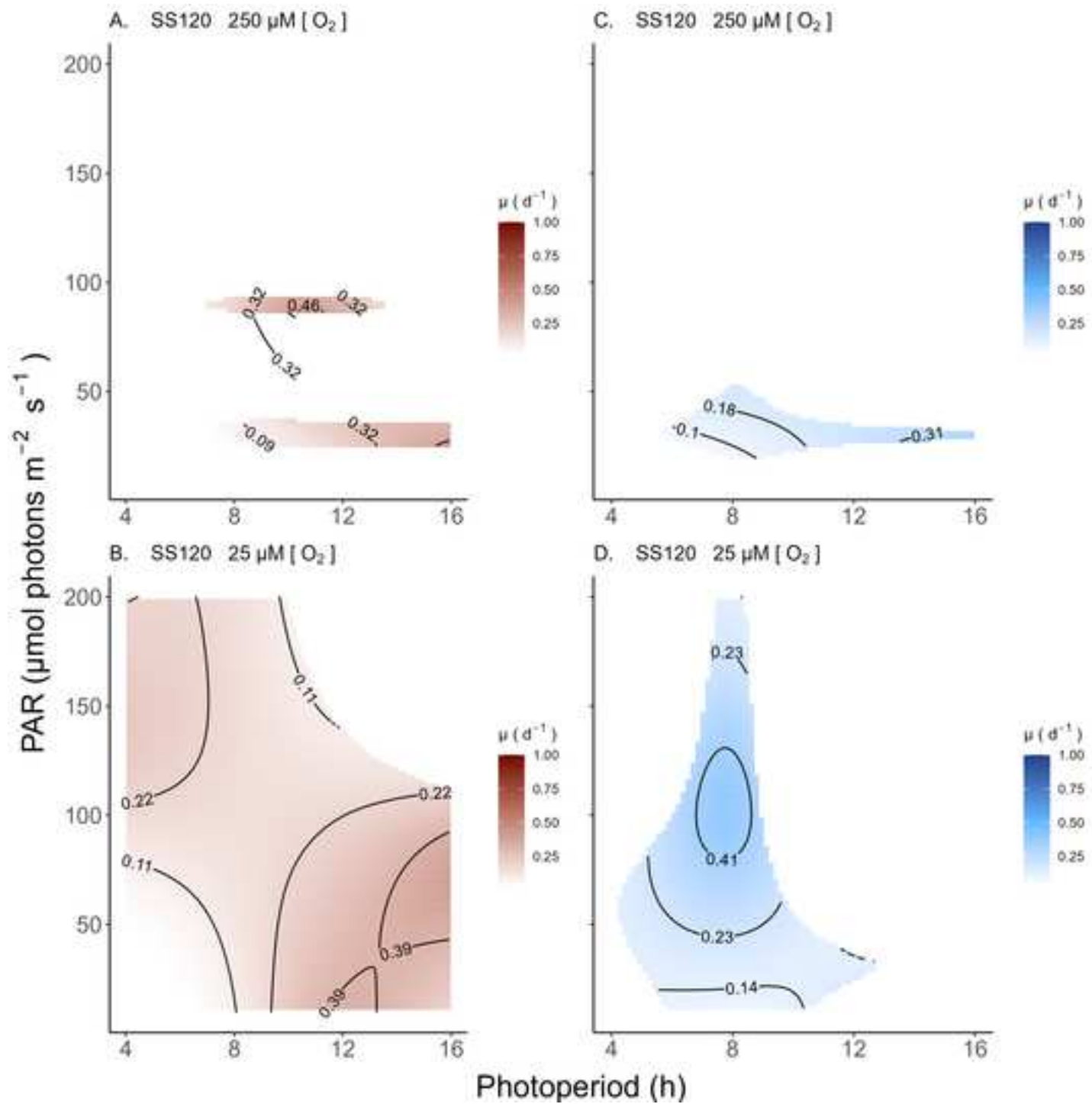
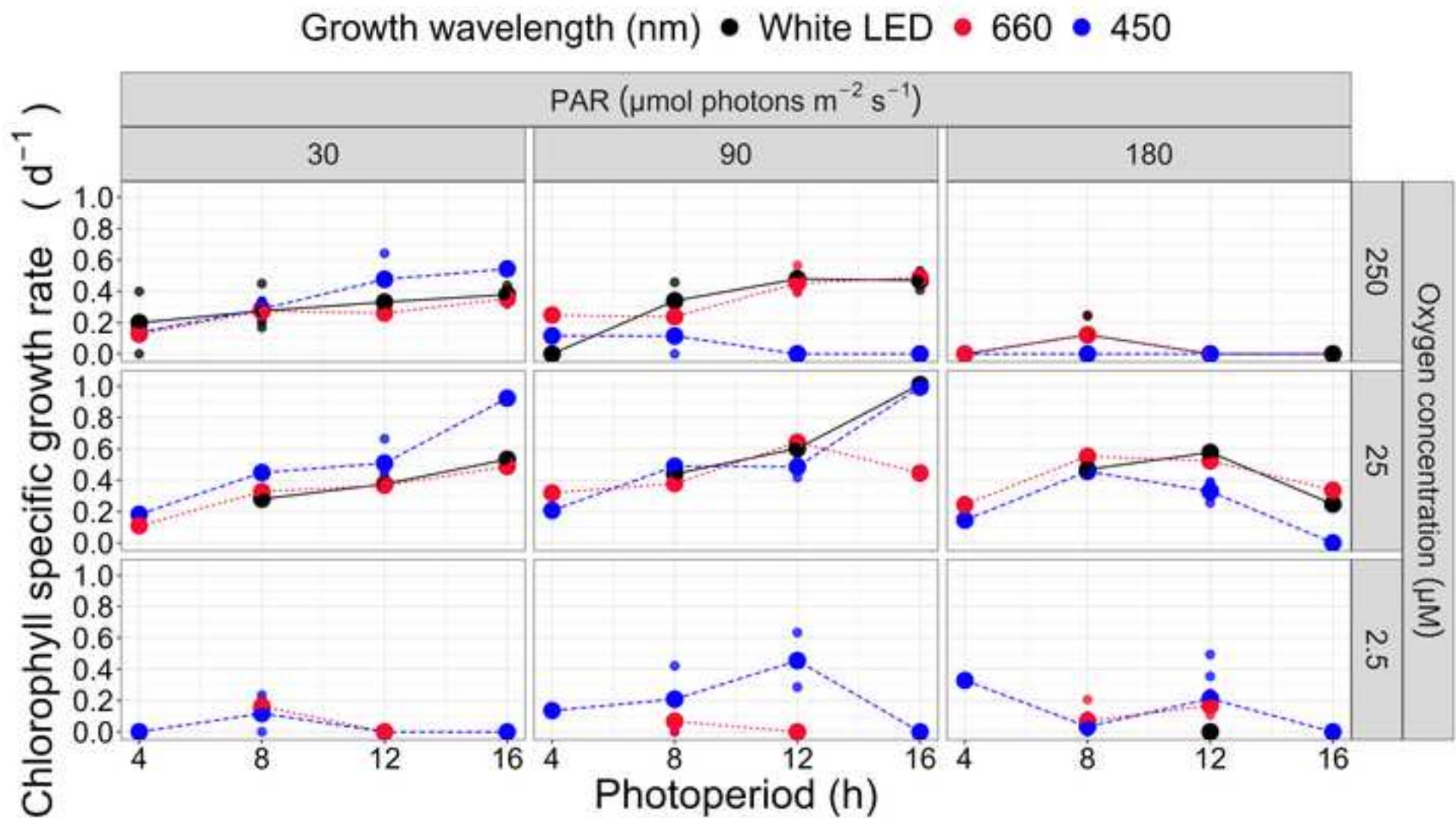
[Click here to access/download/](#)[Figure;Fig6.tif](#)


Figure 7

[Click here to access/download/](#)[Figure;Fig7.tiff](#)

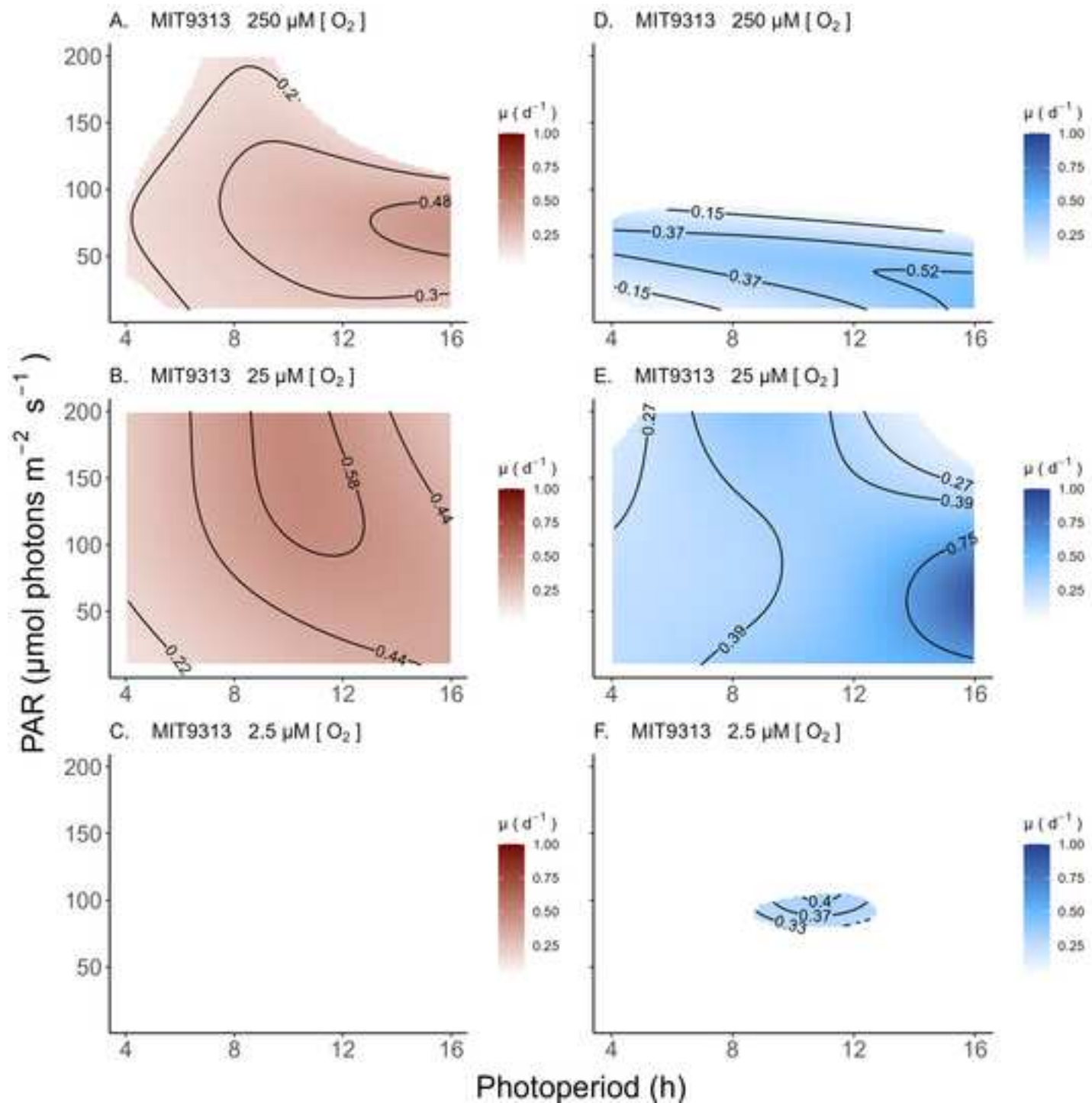


Figure 9

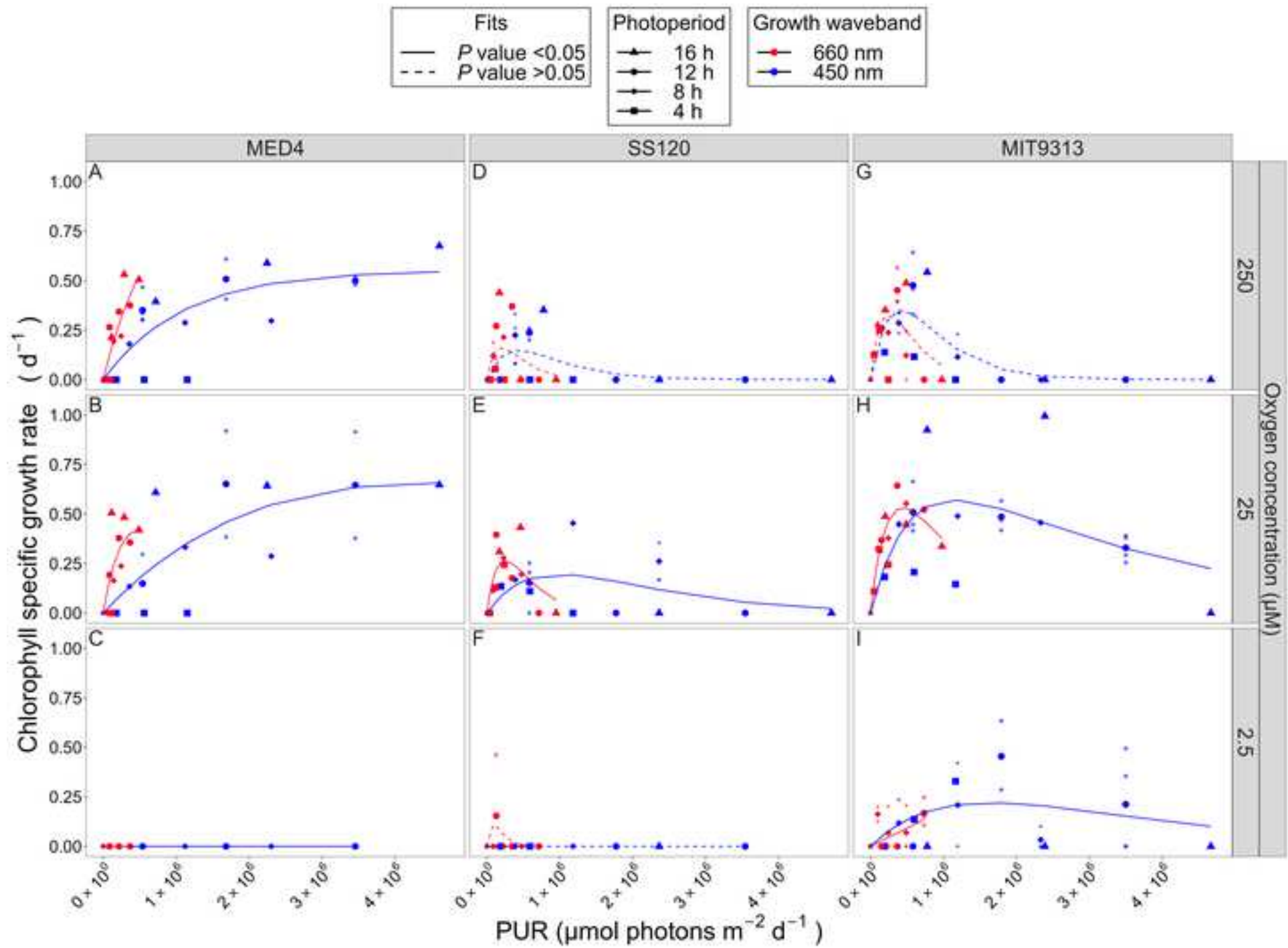
[Click here to access/download/](#)[Figure;Fig9.tif](#)

Figure 10

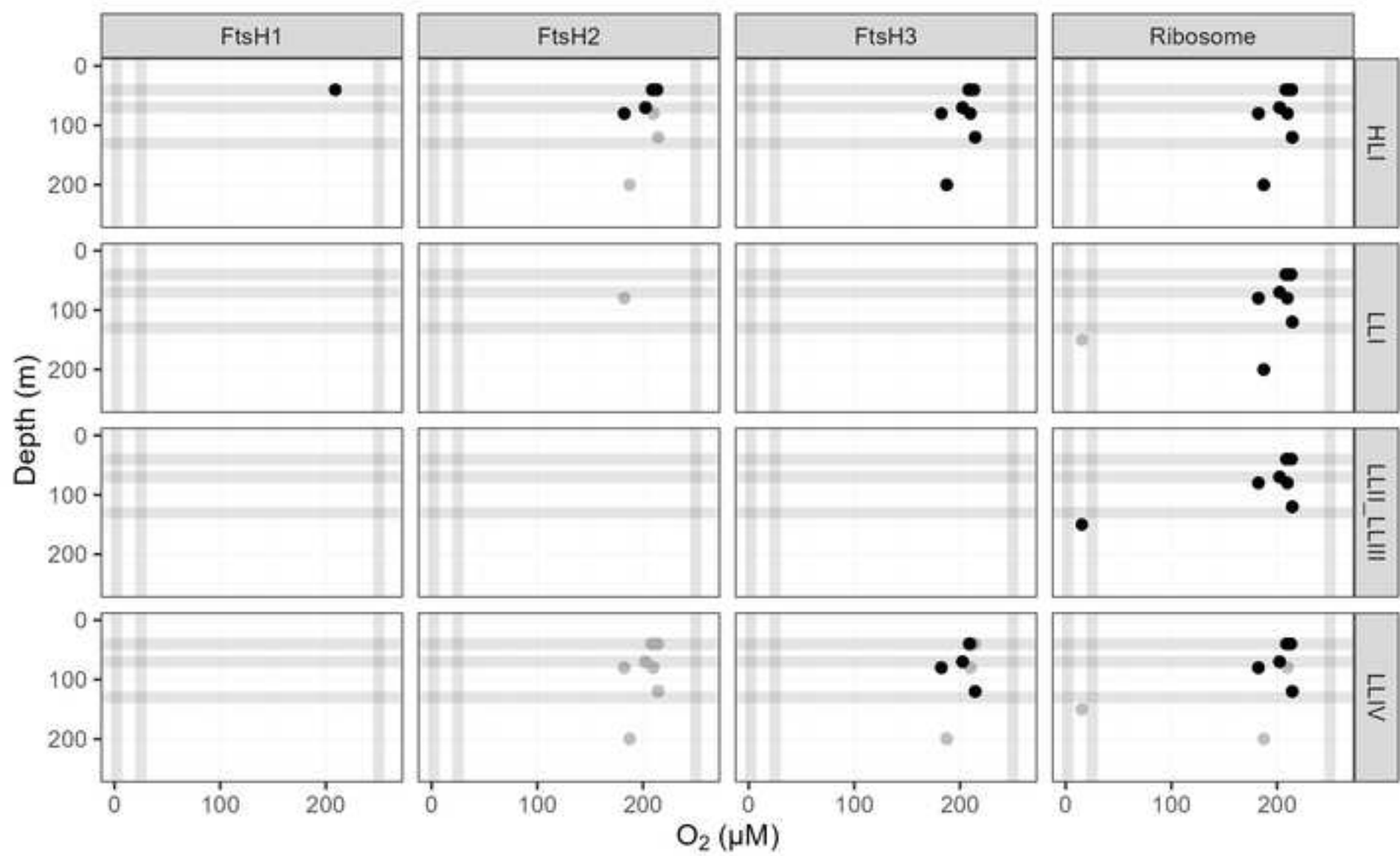
[Click here to access/download;Figure;Fig10.tif](#)

Figure 11

Click here to access/download;Figure;Fig11.tif

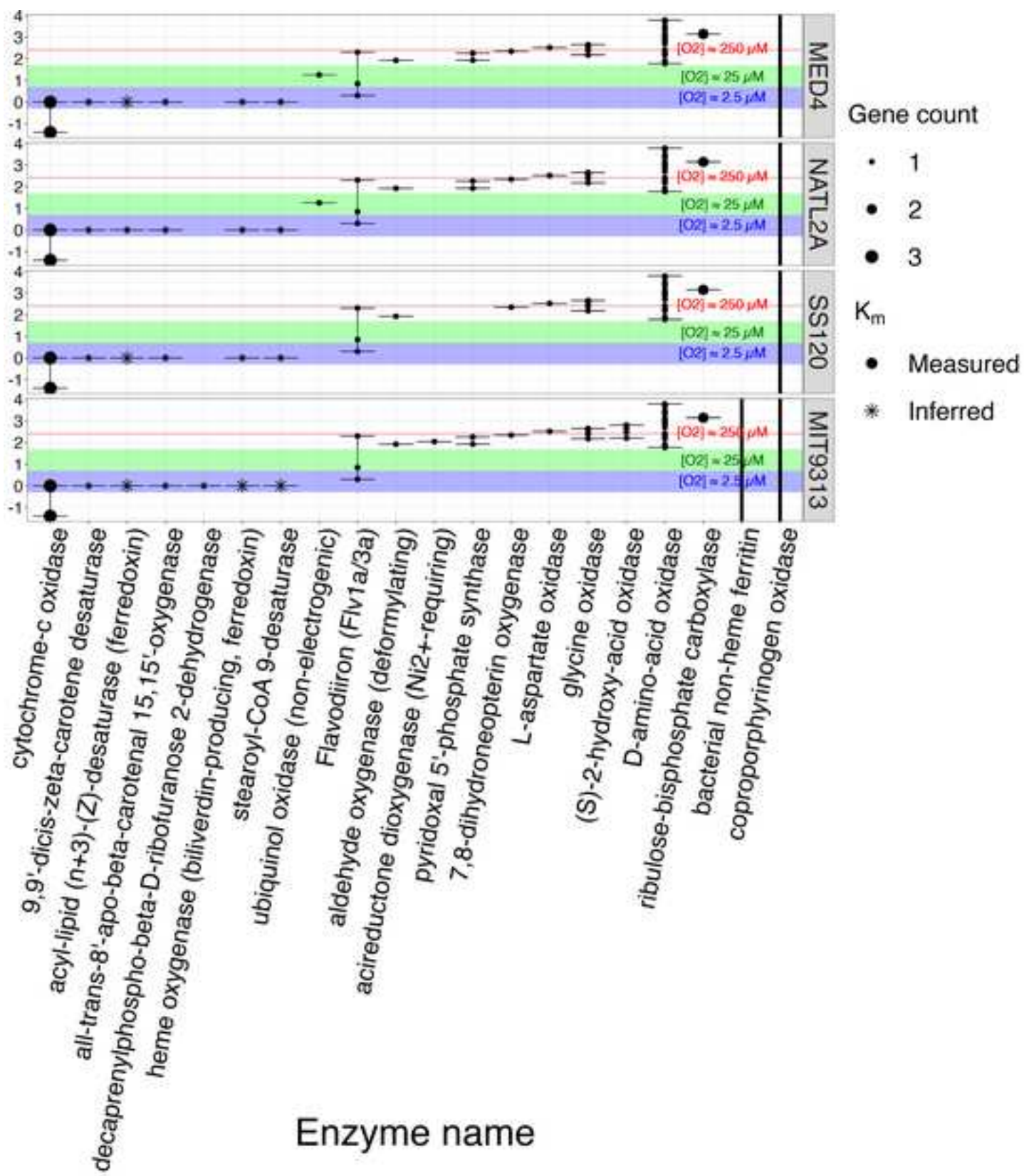


Figure 12

Click here to access/download;Figure;Fig12.tif 